

DUSTY OB STARS IN THE SMALL MAGELLANIC CLOUD - I: OPTICAL SPECTROSCOPY REVEALS PREDOMINANTLY MAIN-SEQUENCE OB STARS

HOLLY A. SHEETS¹, ALBERTO D. BOLATTO¹, JACCO TH. VAN LOON², KARIN SANDSTROM³, JOSHUA D. SIMON⁴, JOANA M. OLIVEIRA², AND RODOLFO H. BARBÁ⁵

¹Department of Astronomy, University of Maryland, College Park, MD 20742-2421, USA; bolatto@astro.umd.edu

²Lennard-Jones Laboratories, Keele University, ST5 5BG, UK

³Max-Planck Institut für Astronomie, Königstuhl 17, D-69117 Heidelberg, Germany

⁴Observatories of the Carnegie Institution for Science, 813 Santa Barbara Street, Pasadena, CA 91101, USA

⁵Departamento de Física, Universidad de La Serena, Cisternas 1200 Norte, La Serena, Chile

Draft version August 7, 2018

ABSTRACT

We present the results of optical spectroscopic follow-up of 125 candidate main sequence OB stars in the Small Magellanic Cloud (SMC) that were originally identified in the S³MC infrared imaging survey as showing an excess of emission at 24 μ m indicative of warm dust, such as that associated with a transitional or debris disks. We use these long-slit spectra to investigate the origin of the 24 μ m emission and the nature of these stars. A possible explanation for the observed 24 μ m excess, that these are emission line stars with dusty excretion disks, is disproven for the majority of our sources. We find that 88 of these objects are normal stars without line emission, with spectral types mostly ranging from late-O to early-B; luminosity classes from the literature for a sub-set of our sample indicate that most are main-sequence stars. We further identify 17 emission-line stars, 7 possible emission-line stars, and 5 other objects with forbidden-line emission in our sample. We discover a new O6 Iaf star; it exhibits strong He II 4686 Å emission but relatively weak N III 4640 Å emission that we attribute to the lower nitrogen abundance in the SMC. Two other objects are identified with planetary nebulae, one with a young stellar object, and two with X-ray binaries. To shed additional light on the nature of the observed 24 μ m excess we use optical and infrared photometry to estimate the dust properties of the objects with normal O and B star spectra and compare these properties to those of a sample of hot spots in the Galactic interstellar medium (ISM). We find that the dust properties of the dusty OB star sample resemble the properties of the Galactic sample of hot spots. Some may be runaway systems with bow-shocks resulting from a large velocity difference between star and ISM. We further investigate the nature of these dusty OB stars in a companion paper presenting mid-infrared spectroscopy and additional imaging.

Subject headings: dust — infrared: ISM — infrared: stars — Magellanic Clouds — planetary systems: formation — stars: early-type

1. INTRODUCTION

The *Spitzer* Survey of the Small Magellanic Cloud (S³MC) carried out deep imaging of the main body of the SMC in all seven IRAC and MIPS bands (Bolatto et al. 2007). This survey identified about 400,000 compact sources in the infrared. Compilation of spectral energy distributions and cross-correlation against optical catalogs uncovered 193 point sources with 24- μ m emission, but with optical and near-infrared colors and magnitudes all consistent with O9–B3 type main-sequence stars. Photospheres of such stars are well below the detection limit of this survey, so an additional source of infrared (IR) emission must be present, presumably warm dust with a temperature close to 150 K. Figure 1 shows the $V, V - I$ color-magnitude diagram for all objects detected at 24 μ m in the S³MC survey, and the box represents the $V - I$ and M_V cuts on the dusty OB star sample. These sources are a puzzle, representing a few percent of all the stars in that particular color and magnitude range in the SMC. Dust in close proximity to an early B/late O star could be a remnant from the accretion process, and provide important information about the final stages of accretion and the clearing up of the original disk in massive stars. We discuss below several

competing possibilities for the nature of these sources, previously presented by Bolatto et al. (2007). The discovery of these objects has been confirmed independently by the *Spitzer* SAGE-SMC survey (Bonanos et al. 2010, who also discuss them) and by Ita et al. (2010) using AKARI data.

If the dust is associated with the star, it must exist either in an optically thin shell surrounding the star or in a thin or transition circumstellar disk, since no appreciable reddening of the central star is detected beyond the line-of-sight extinction by our own Galaxy to the SMC. These objects have $F_{IR}/F_{Bol} \sim 10^{-4}$ to 10^{-2} , indicating that the dust is intercepting only a small fraction of the star's light and re-radiating it in the IR. This also supports the thin shell or disk scenario. Since most of the dusty OB stars show little to no excess emission at wavelengths of 8 μ m or shorter, a large central gap would be needed to explain the absence of significant emission from hotter dust located close to the star.

A clump of interstellar dust, heated by a nearby star, however, could also reproduce these characteristics. This is observed, for example, in the Pleiades (Arny 1977; White & Bally 1993; Herbig & Simon 2001; Sloan et al. 2004). Vega-like stars, Herbig Ae/Be stars, and classical

Be stars all have disks that are known to contain dust to varying degrees, and so we consider them, as well as cirrus hot spots in the ISM, as the possible causes for the excess emission seen around these O and B stars in the S³MC survey.

Vega-like stars host debris disks, which are the remnants of planet formation. They are optically thin dust disks, mostly stripped of their primordial gas and continually replenished by collisions between planetesimals. The prototypical examples are Vega, Fomalhaut, and β Pictoris, all of which have disks that extend 100 to 1000 au from the star with $L_{IR}/L_{Bol} \sim 10^{-5}$ to 10^{-3} (Backman & Paresce 1993, and references therein). The central region, a few au in extent, of these disks has been cleared of dust, just as in our solar system, and the mass of emitting dust is $\sim 10^{-3}$ to $10^{-2} M_{\oplus}$ at temperatures between 50 and 125 K. The wider sample of debris disks shows an upper limit on F_{IR}/F_{Bol} of 10^{-2} (Chen et al. 2006), temperatures up to 300 K, and dust masses as large as an Earth mass (Krivov 2010). Note however that the known debris-disk hosts are observed, overwhelmingly, around much less massive stars with later spectral types. A gas-free disk around a very luminous star would be quickly cleared by radiation pressure, unless the dust grains are very large.

Classical Be stars are rapidly rotating main-sequence stars with an excretion disk of gaseous material (Porter & Rivinius 2003). The disk produces IR excess in the form of free-free emission with approximately $S_{\nu} \propto \nu^{0.6}$ in the near- and mid-IR (Waters & Marlborough 1994); this by itself would not explain the sudden rise observed in the spectral energy distribution (SED) of the dusty O and B stars at 24 μ m. Miroschnichenko & Bjorkman (2000), however, found evidence for circumstellar, thermal dust emission in some Be stars in the far-IR, which they attribute to remnant dust from prior evolutionary processes.

Herbig Ae/Be stars, on the other hand, are pre-main sequence stars that are thought to be the more massive analogs to T Tauri stars. They are surrounded by gaseous accretion disks containing dust with temperatures as high as 1500 K, creating the IR excess (see, e.g. Hillenbrand et al. 1992; Waters & Waelkens 1998). Herbig Ae/Be stars typically show significant excess at $\lambda \geq 1 \mu$ m from this hot dust. The onset of the emission at longer wavelengths indicates that the central portion of the disk nearest the star has been cleared and is free of dust. Disks with such a central hole are transition disks (e.g., Cieza et al. 2010). It is possible that more massive, early-B and O stars also go through this stage, although modeling suggests that this may be an exceedingly short phase as disks are rapidly cleared (Alexander et al. 2006). Observational evidence for circumstellar disks around massive B and O stars remains hard to come by (Cesaroni et al. 2007).

The Galactic cirrus, comprised of wispy or filamentary patches of dust throughout the disk of the Galaxy, has a typical temperature of ~ 18 K (Planck Collaboration et al. 2011), but heating of the cirrus by embedded stars produces small regions of warmer dust, or hot spots, near the star, reaching temperatures of ~ 70 K (van Buren & McCray 1988). It is difficult to distinguish debris disks from hot spots in the cirrus without resolved images of either the dust

emission in the IR, or the scattered light in the optical. The observed SEDs can be interpreted with either scenario, as illustrated by Martínez-Galarza et al. (2009) and Su et al. (2006); Martínez-Galarza et al. model some of the same objects in Su et al. as ISM heated by stars passing through a cloud, while Su et al. model them as debris disks. Cirrus hot spots are also sometimes the cause of the far-IR emission detected around Be stars (Miroschnichenko & Bjorkman 2000).

Understanding the source of the excess emission in these objects is valuable because the scenarios above represent different phases in the evolution of massive stars. Detecting circumstellar material around SMC stars is interesting, because it offers the opportunity to study accretion or excretion processes in a low metallicity environment, and particularly around massive stars with an unextincted line-of-sight. Detecting debris disks in the SMC would be especially exciting, as they would offer an unprecedented opportunity to study planet formation in another galaxy. Such early-type stars are under-represented in Galactic studies.

While the photometry suggested the stellar counterparts of the IR emission to be early-type main-sequence stars, this has yet to be confirmed through spectroscopic observation. The vast majority of the 193 objects in our sample do not have spectral types reported in the literature, although a small subsample has fiber optics spectroscopy (Evans et al. 2004).

Bonanos et al. (2010) compiled a catalog of IR counterparts to massive stars spectroscopically confirmed in the literature. They identify 44 objects that are similar (OB stars with 24 μ m emission) but not necessarily identical to our sample. They constitute $\sim 2\%$ of their sample of late-O and early-B stellar types, a fraction slightly lower but otherwise similar to that reported by Bolatto et al. (2007). The 18 spectra Bonanos et al. have in hand show nebular line emission, unlike — as we shall see — the majority of the sources in this sample. Note that the spectra used by Bonanos et al. are obtained using fibers (Evans et al. 2004, 2006), which makes sky subtraction in complex regions problematic. Long-slit spectroscopy is preferred in regions of diffuse sky emission such as found around massive stars. Clearly, further spectroscopic study is warranted. Bonanos et al. (2010) conclude that most of their sources are not found within very young regions, and suggest their IR emission is likely dust associated with cirrus or a nearby molecular cloud, rather than disks. Bolatto et al. (2007), however, noted that the majority of the sources identified in their sample are in the vicinity of active star-forming regions although not in their cores, where confusion with diffuse 24 μ m emission would make their identification extremely difficult.

We obtained optical long-slit spectroscopy for 125 of the 193 objects from the S³MC survey in order to determine how many of them are emission-line (e.g., classical Be and Herbig Ae/Be) stars and to obtain spectral types to quantify the stellar radiation field illuminating the dust. In section 2 of this paper, we discuss the photometric and spectroscopic observations, while in section 3 we classify the stars, and in section 4 we estimate the properties of the dust around the non-emission line objects. In section 5, we discuss how well the various scenarios explain our objects and include a comparison of

the dust properties to those estimated from the sample of Galactic cirrus hot spots of Gaustad & van Buren (1993). In a companion paper (Adams et al. 2013, hereafter Paper II), we discuss further infrared spectroscopic and photometric information, and comparisons to large Galactic samples based on *Wide-field Infrared Survey Explorer* (WISE) data.

2. OBSERVATIONS

2.1. Spectroscopy

The optical spectra were obtained at the 3.5-m New Technology Telescope at the European Southern Observatory at La Silla, Chile in 2007 September (programme 079.C-0485; PI J.Th.van Loon), using the EMMI instrument (Dekker et al. 1986) in RILD mode in the red arm with grism #2 and a $1''.0$ slit. This set-up provided wavelength coverage from ~ 385 to 870 nm with $\lambda/\Delta\lambda = 570$. Biases, dome flats, and HeAr arc lamp frames were acquired for calibration. The science integrations were split into three exposures, offset along the slit, in order to correct for cosmic rays and fringing effects at wavelengths beyond 750 nm). A filter to block second-order contamination longward of 800 nm was originally planned, but it was dropped because of unwanted reduction of signal in the blue region of the spectrum.

The spectra were wavelength-calibrated with HeAr lamp exposures, using the IRAF¹ IDENTIFY, REIDENTIFY, and TRANSFORM tasks in the NOAO spectroscopic reduction package. The 1D spectra were then extracted using the APSUM task. The extraction was at times complicated by the background emission lines from H II regions within which our targets were located. To remove this background, the aperture and background regions were set interactively, looking first at the profile of the star along the slit, away from any emission lines. If any [O III] 5007 Å emission remained in the extracted spectrum, the extraction was re-done looking instead at the profile along the slit at the [O III] line to set the aperture and background regions. The extracted spectra were summed for each object to increase the number of counts and to average out fringing effects and an electronic interference pattern that could not be removed with the bias or dark frames due to frame-to-frame variations. Lastly, the spectra were normalized to the continuum in the region between 400 and 680 nm by fitting and dividing by an order 20 polynomial.

2.2. Photometry

The photometry used to create the SEDs for each source is a combination of B , V , and I data from the OGLE II survey (Udalski et al. 1998) and the Magellanic Clouds Photometric Survey (Zaritsky et al. 2002), J , H , and K_s from the 2MASS survey (Skrutskie et al. 2006), and *Spitzer* Space Telescope (Werner et al. 2004) data from both the original S³MC (Bolatto et al. 2007) survey and the combined S³MC/SAGE-SMC catalogs (Gordon et al. 2011), making use of the IRAC (Fazio et al. 2004) and MIPS (Rieke et al. 2004) instruments. In the SAGE-SMC processing, combined S³MC/SAGE-SMC images were created by stacking data

from both surveys before performing the photometry. For the MIPS combined catalog, on the other hand, photometry was performed on the three different observing epochs (one for S³MC, and two for SAGE-SMC) separately, after uniformly reprocessing the data. We searched the combined catalogs for coordinate matches to the dusty OB stars within $2''$. The IRAC and 2MASS data points in the original S³MC photometry were replaced with the points in the combined catalog if they existed. If more than one match was found, the closest match was used. The 24 μm points in the original S³MC catalog were replaced with the weighted average of the three epochs in the combined catalog for the closest positional match. Points were replaced as long as there was a match within $2''$ in at least one of the epochs. The 70 μm data points, where they exist, must be treated with caution. The diffuse emission in the SMC is considerably brighter at 70 μm than at 24 μm , and the difference in beam size between the two channels is substantial. The beam size at 24 μm is $6''$, corresponding to 2 pc at the SMC distance of 61.1 kpc (Keller & Wood 2006), while the beam size at 70 μm is $18''$, corresponding to 5 pc. Thus there is a good chance of source confusion between the two channels, and we have not searched the combined S³MC/SAGE-SMC catalog for 70 μm matches. The photometry data are given in Tables 1 and 2.

3. SPECTRAL CLASSIFICATION

We use our long-slit spectroscopy to classify the stars. For the classification, we employ the scheme described in Evans et al. (2004), which compares the strengths of a number of lines in the 4000 – 5000 Å range. We use the equivalent widths of the lines, guided by visual inspection of the spectra, to compare the line strengths, but our low resolution leaves some of the important lines blended with H δ (Si IV 4088 Å and Si IV 4116 Å) or with each other (e.g., He I 4471 Å and Mg II 4481 Å). Note also that the original classification scheme was designed for supergiants, and so the Si lines for main-sequence stars may be too weak to detect in some cases. The classification scheme is summarized in Table 3. A sample spectrum of object B 107 is shown in Figure 2. Since B 107 shows no He II absorption features, it is not an O star. It shows no evidence of Si III 4553 Å, so it is not a B2 or B3, but the Mg II 4481 Å appears too weak for a spectral type later than B3. Thus we conclude that most likely the Si IV lines are blended with H δ and that the star is a B1.

Of the 125 objects for which we obtained spectra, 87 appear to be normal main-sequence stars and one (B 167) is discussed below as a likely supergiant. Of those 87, 53 are classified via the above scheme and assigned a subtype. The remaining 34 stars were difficult to place precisely within the scheme, but they have been marked as either O7–O9, if they show He II absorption, or B0–B2 if they lack the He II lines. B 167 is unusual, however, in that it shows no significant He I absorption but has very strong Balmer absorption. It appears to be an A star; given its luminosity it is probably a supergiant. The spectra and SEDs of these 88 objects are shown in Figures 3 through 8, while the assigned spectral type is given in Table 4 as well as in the figures.

The remaining 37 of the 125 objects, which are not considered in the dust analysis in the next section, fall into

¹ IRAF is distributed by the National Optical Astronomy Observatories.

one of four groups: 1) stars that show Balmer emission and sometimes He I/II emission (16 stars plus B 094), 2) stars with unusual H α profiles (7 stars, including B 035 which we specifically discuss in the following section), 3) objects that show strong forbidden line emission (6 objects), and 4) spectra that are difficult to extract (8 stars).

The first group of 17 stars shows the Balmer and He I/II emission lines characteristic of Be stars (Figure 9), while the second group of 7 stars shows only weak H α absorption (Figure 10). B 094 stands out, as it is the only object among the 17 stars that shows [N II] $\lambda\lambda$ 6548,6583 emission. We include it here, rather than with the strong forbidden-line emission objects, because of the lack of [O III] emission and the weakness of the Balmer emission compared to the other objects in that group. The unusually weak Balmer absorption in the second group of stars may indicate that these objects are Be stars as well. Silaj et al. (2010) modeled the H α profiles of Be stars and showed that, for many combinations of base-disk density, density distribution, and viewing angle, the H α emission from the circumstellar matter does not cancel out the absorption line of the star completely. This effect could explain the unusual H α profiles. The definite Be stars are noted with a spectral type of OBe in Table 4, while stars with possible weak emission are noted as “OBe?” in the table.

The third group is comprised of 6 objects (5 shown in Figure 11, plus the already discussed B 094), and it includes B 001, B 028, and B 079, all of which show strong Balmer and [O III] $\lambda\lambda$ 4959,5007 emission, along with weaker [N II] $\lambda\lambda$ 6548,6583 and He II $\lambda\lambda$ 5876,4921, and 4471 Å emission. These spectra are typical of compact H II regions. B 141 is dominated by Balmer emission, with weak [N II] and very weak He I emission. B 141 also shows moderate [O III] emission, but unlike B 001, B 028, and B 079, the forbidden-line emission is weak relative to H β . B 036 is now known to be a young stellar object (YSO) (Oliveira et al. 2013); it shows strong Balmer emission, with weak [N II] emission, very weak [O III] emission, and little to no He I emission above the continuum level. The SEDs of these five sources are much flatter than those of the non-emission-line objects, possibly due to the predominance of the free-free emission over any stellar photospheric emission. These objects are marked in Table 4 as Em in the spectral type column.

The fourth group, shown in Figure 12, includes B 005, B 011, B 112, and B 175, all of which have low signal-to-noise spectra and, except for B 011, also have a star too nearby to set the background well. Thus it is unclear whether the H α absorption appears weak because of noise, background contamination, or weak Be star emission. The other 4 objects in this group are B 006, B 093, B 108, and B 191, whose complicated background in H α makes it difficult to disentangle emission from the surrounding nebula from possible Be star emission. These objects are given no spectral type in Table 4.

3.1. A newly discovered O6 Iaf star

In the “OBe?” group, B 035 is the only star that shows He II 4686 Å emission. The spectrum is displayed in more detail in Figure 13. The appearance of the He II 4686 Å emission indicates a very high luminosity, class

Ia (Sota et al. 2011). This is commonly accompanied by emission of the N III 4640 Å complex, but this is weak in the spectrum of B 035. We suggest that this is a metallicity effect due to the low nitrogen abundance in the SMC (van Loon et al. 2010). It does appear to be present, hence we tentatively affix the “f” suffix to the spectral type. With regard to the temperature class, the He I 4471 Å/He II 4200 Å ratio suggests a spectral type of about O6 (Sota et al. 2011). The He I+II 4026 Å line is weaker than that of the He II 4200 Å line, which would suggest a spectral type < O4, but it is also weaker than that of the He I 4471 Å line, which would suggest a spectral type > O7 (which does not really happen, Sota et al. 2011) – we attribute this to uncertainties and/or possible binarity and arrive at a final spectral classification of O6 Iaf.

3.2. Comparison with literature

Accurate spectral classification based on high quality data was carried out by Evans et al. (2006), Martayan et al. (2007), Evans & Howarth (2008) and Hunter et al. (2008) for 23 of our 125 stars (see Table 4). Our own spectral classifications are in agreement with those determinations, with only a few deviations by one or two subclasses. The majority (~ 14) of those classifications are of luminosity class IV–V, with only 6 of luminosity class II and none more luminous. This suggests that most of the stars in our sample are unevolved, main-sequence stars.

The sample, however, is a mixed bag of curious and seemingly very common types of objects. The “Em” objects include the planetary nebulae B 001 = LHA 115-N9 and B 079 = LHA 115-N47, the YSO B 036 (Oliveira et al. 2013), and the compact H II region B 028 = LHA 115-N26 (Testor 2001). The sample further includes the X-ray binaries B 064 = SXP 214 (Coe et al. 2011) and B 085 = CXOU J005245.0–722844 (Antonioni et al. 2009) and no less than 10 or 11 eclipsing binaries. We attribute the large number of eclipsing binaries to the high overall fraction of close binary systems among massive stars (Sana et al. 2012, 2013).

4. CONSTRAINING THE DUST PROPERTIES

In order to assess the viability of the various hypotheses for the nature of the dusty OB stars and the origin of the dust, we now use the available photometry to estimate the gross properties of the dust. The primary quantities we can constrain are the dust temperature, dust mass, the fraction of the star’s light re-radiated by the dust (F_{IR}/F_{Bol}), and the distance of the dust from the star. We also calculate the grain size below which radiation pressure will quickly remove the dust from the system in the absence of gas drag, as well as the mass of grains of that blow-out size that would be needed to account for the observed F_{IR}/F_{Bol} .

To determine these properties, we first find the amount of expected flux from the stellar photosphere by fitting to the SED a power law of the form

$$\ln(\nu I_\nu) = m \ln(\lambda) + b \quad (1)$$

with ν in Hz and λ in μm , and with the slope m derived from the Kurucz stellar atmosphere model

(Castelli & Kurucz 2003) of the spectral type determined. The intercept b was determined using the J -band flux, or I if J was unavailable, to scale the models. The J and I fluxes were corrected for the line-of-sight extinction due to the Milky Way using $A_I = 0.482A_V$ and $A_J = 0.282A_V$ from Draine & Lee (1984) and Rieke & Lebofsky (1985), with $A_V = 0.12$ mag (Schlegel et al. 1998). We selected models for $[M/H] = -0.5$, closest among the Kurucz library to the typical abundance of young stars and gas in the SMC of $[M/H] \sim -0.7$ (Pagel et al. 1978), and the suggested surface temperatures and surface gravities for specific stellar types from Martins et al. (2005) and Schmidt-Kaler (Aller et al. 1982). All the fits used models with $\log g = 4$ for the surface gravity, and the surface temperature and slope used for each spectral type is given in Table 3. The temperature scale is similar – well within 10% – to that of Galactic main-sequence stars determined by Nieva (2013) and that of O-type stars in the SMC determined by Massey et al. (2005); the latter found that early-O type stars in the SMC are hotter than Galactic stars of the same spectral type, but that this difference vanishes around B0. A slope $m = -2.91$ was used if the star was given a spectral type of “O7–O9”, while a slope $m = -2.84$ was used for all other stars without a specific spectral type. From these fits, the excesses at 4.5, 8, and 24 μm were calculated (Table 5), along with the ratio of the excess to the expected photosphere.

4.1. Dust Temperature

In all but six cases, marked with a footnote in Table 5, no emission was detected at 70 μm , so we cannot fit a model to the 8, 24, and 70- μm excesses directly. Instead we estimate the color temperature of the dust using the 8- and 24- μm excesses, and place limits on the color temperature using the 24 μm flux and the 70 μm flux limit of 40,000 μJy , minus the expected photospheric flux. The color temperatures are estimated assuming a modified blackbody with emissivity $\propto \lambda^{-2}$, using the equation

$$\frac{f_a}{f_b} = \left(\frac{\lambda_b}{\lambda_a} \right)^5 \frac{\exp(hc/\lambda_b kT) - 1}{\exp(hc/\lambda_a kT) - 1}, \quad (2)$$

where a is the shorter wavelength and b the longer. The color temperatures calculated for the ratios of the 8- to 24- μm excesses, for stars with a specific spectral type, are given in Table 6. Because the 8- μm band includes a major polycyclic aromatic hydrocarbon (PAH) feature, these color temperatures must be treated with caution. Note, however, that PAH emission in the SMC is considerably weaker than in the Milky Way making this less of a problem than for local samples (Sandstrom et al. 2010). The color temperatures calculated with the 24- to 70- μm ratios are very uncertain, since in most cases we have only an upper limit on the 70- μm flux, and thus are not included in the table. These values are generally in the range of 40–60 K, but they should be considered as lower limits as a 70- μm flux below the upper limit would lead to a higher derived temperature. Mid-IR spectroscopy and deeper 70- μm photometry to determine the dust temperature directly are presented in Paper II.

4.2. Dust Mass

We are working in the optically thin limit at long wavelengths, so the emission of the dust is given by

$$I_\nu = \Omega \tau_\lambda B_\nu, \quad (3)$$

where I_ν is the excess emission at 24 μm , Ω is the solid angle subtended by the source, τ_λ is the opacity due to the dust, and B_ν is the emission of a blackbody at the temperature of the dust. The opacity of the dust is

$$\tau_\lambda = \frac{M_d}{\Omega D^2} \kappa_\lambda, \quad (4)$$

where M_d is the mass of the dust, ΩD^2 is the area covered by the dust, and κ_λ is the dust mass absorption coefficient. Thus the dust mass is given by

$$M_d = \frac{I_\nu D^2}{\kappa_\lambda B_\nu}. \quad (5)$$

Here we assume

$$\kappa_\lambda = 10 \left(\frac{250}{\lambda} \right)^2, \quad (6)$$

where κ_λ has units of $\text{cm}^2 \text{g}^{-1}$ and λ is given in μm . This value is due to Hildebrand (1983) and within 20% of Draine & Lee (1984). We adopt it to be easily comparable to surveys of the Milky Way (for example, the Gould Belt Survey; André et al. 2010). The dust mass then is

$$M_d = 3.9 \times 10^{-23} \frac{I_\nu D^2 \lambda^2}{B_\nu} M_\oplus, \quad (7)$$

where I_ν is given in mJy, D in pc, λ in μm , and B_ν in $\text{erg cm}^{-2} \text{s}^{-1} \text{Hz}^{-1} \text{sr}^{-1}$. The dust masses calculated using temperatures the derived from 8/24- μm excess ratios are listed in Table 6.

4.3. Dust Luminosity

To calculate the fractional luminosity F_{IR}/F_{Bol} , we first determined the infrared flux by integrating over the source function for graybody emission from 0.7 μm to 100 μm , rewriting Eq. 3 above as

$$I_\nu = 3.18 \times 10^{-4} \frac{M_d}{D^2} \frac{1}{\lambda^2} B_\nu, \quad (8)$$

where M_d is in M_\oplus , D is the distance to the source in pc, λ in μm , and I_ν in $\text{erg cm}^{-2} \text{s}^{-1} \text{Hz}^{-1}$. We then divided by the bolometric flux, which is the luminosity for the spectral type (Table 3), scaled to the distance of the SMC.

4.4. Distance of the Dust from the Star

The observed dust temperature and stellar luminosity constrain the location of the dust in the circumstellar environment. The distance of the dust from the star at a given temperature also depends on the size of the dust grains and the wavelength range of the light being absorbed. We can set limits on the dust distance by first assuming the relation for large, blackbody grains,

$$R_{BB} = 2.32 \times 10^{-3} R_\star \left(\frac{T_\star}{T_{dust}} \right)^2, \quad (9)$$

where R_\star is the stellar radius in units of R_\odot and R_{BB} is the dust distance in au. The stellar radii for the stars

are given in Table 3 and are taken from a second-order polynomial fit in T to the values given in Appendix E of Ostlie & Carroll (1996). The distances calculated with this model are given in Table 6 as the blackbody (BB) distance. Grains that instead absorb light as blackbodies, but re-radiate as a modified blackbody proportional to λ^{-2} , can be modeled using the equation

$$R_{\text{MBB}} = 636^3 \frac{\sqrt{L_\star}}{\lambda_0 T_g^3}, \quad (10)$$

where L_\star is in L_\odot , R_{BB} is in au, and λ_0 is in μm . This equation is taken from Equation 2 of Backman & Paresce (1993), assuming $p = 0$ and $q = 2$. We have assumed $\lambda_0 = 1 \mu\text{m}$. Note that this last parameter is poorly constrained and it introduces significant uncertainty in R_{MBB} . The distances calculated with this model are listed in Table 6. Smith & Wyatt (2010) note that in resolved debris disks, the actual distances of the particles are at most 3 times the distance predicted by the blackbody grain model, whereas in resolved cirrus hot-spots, the dust distance is an order of magnitude – or more – larger than that expected from the blackbody model, due to stochastic heating of small grains (Kalas et al. 2002).

We also estimate the blow-out size for grains due to radiation pressure in the absence of gas drag. Grains with $\beta = F_{\text{rad}}/F_{\text{grav}} > 1$ will be blown out of the system by radiation pressure. We use the equation for β from Burns et al. (1979),

$$\beta = 0.57 Q_{\text{pr}} \frac{L/L_\odot}{M/M_\odot} \left(\frac{a}{\mu\text{m}} \right)^{-1} \left(\frac{\delta}{\text{g cm}^{-3}} \right)^{-1}, \quad (11)$$

where a is the size of the grain, δ is the density of the grain, and Q_{pr} is the average radiation pressure efficiency over the stellar spectrum for a given grain size. Values for L for the spectral types are given in Table 3 and were derived using

$$\frac{L}{L_\odot} = \left(\frac{R}{R_\odot} \right)^2 \left(\frac{T}{T_\odot} \right)^4, \quad (12)$$

where $T_\odot = 5780 \text{ K}$ from Schmidt-Kaler (Allen 1973). Values for M were derived by fitting a second-order polynomial in T in logarithmic space to the values in Appendix E of Ostlie & Carroll (1996) and are also given in Table 3. We assume here $Q_{\text{pr}} = 1$, and we use $\delta = 3.3 \text{ g cm}^{-3}$ from the Draine & Lee (1984) model. Setting $\beta = 1$ gives the minimum grain size in a circular orbit that can survive the radiation pressure of the host star. Grains released from parent bodies in circular orbits, such as dust created in a debris disk, however, can be ejected from the system for β as low as 0.5.

We then estimate the mass of dust needed to produce the observed $F_{\text{IR}}/F_{\text{Bol}}$, based on the estimated blow-out size of the grains. This mass (in units of g) is given by

$$M_{\text{bo}} = \frac{16\pi}{3} \frac{F_{\text{IR}}}{F_{\text{Bol}}} \delta a_{\text{min}} R_{\text{BB}}^2, \quad (13)$$

where a_{min} is the minimum grain size to survive radiation pressure blow-out, in cm, and R_{BB} is the blackbody distance in cm.

4.5. Uncertainties

We estimate the uncertainty on these parameters for the 8/24 pair of excesses using the Monte Carlo method. For each of 1000 trials per object, the color temperature is calculated, and that temperature is used in the calculation of the dust mass, $F_{\text{IR}}/F_{\text{Bol}}$, and dust distance. The uncertainties on the color temperature, dust mass, $F_{\text{IR}}/F_{\text{Bol}}$, and dust distance are then set according to the upper and lower values that bracket the central 67% of the results for each object. Uncertainties on the excess at 8 and 24 μm are determined via error propagation, assuming an uncertainty in slope m of 0.05 for B stars and 0.01 for O stars. These ranges allow for uncertainty in the spectral type. Because the O stars all have a similar slope, the range is much smaller. We apply these uncertainties to the excesses assuming a normal distribution about the value of the excess before calculating the color temperature. The dust mass calculation also includes an uncertainty in the distance to the stars, which we model as a normal distribution centered at $61.1 \pm 6 \text{ kpc}$, assuming that the objects are most likely to be located near the center of the SMC. The $F_{\text{IR}}/F_{\text{Bol}}$ calculation further requires the uncertainty on the bolometric luminosity, assumed to be a uniform distribution with a range set by the value for ± 1 spectral sub-type. For the distance calculation, we assume uncertainties for the stellar radius and stellar temperature uniformly distributed between the values for ± 1 spectral sub-type. Table 6 gives the dust parameters for those objects in Table 5 that have a measurable excess at 8 μm , and to which we give a secure main sequence spectral classification.

5. DISCUSSION

5.1. Classical Be Stars

Because the majority of our sample shows no optical emission lines, Be star activity is likely not the main cause of the 24- μm excess in these O and B stars. It is possible, however, that a few of the objects without emission lines could still be Be stars, as Be stars are known to show variability in their Balmer emission. In a study of 45 Milky Way Be stars, McSwain et al. (2009) found 23 objects with variable $\text{H}\alpha$ emission, including six that changed from strong emission to normal B-star absorption at $\text{H}\alpha$ or vice versa over the course of just two years. Of the original sample of 193 O and B stars with 24- μm excess identified in the S³MC survey, 12 were previously catalogued as Be stars by Meyssonnier & Azzopardi (1993), and for those we did not acquire new spectra. We identify here an additional 16 stars with confirmed $\text{H}\alpha$ emission and 7 stars with suspected weak $\text{H}\alpha$ emission, for a total of 35 Be stars (36 if we include B 097 in the count). The remaining 88 stars in the spectroscopic sample do not display evidence of OBe activity.

To investigate the possibility of variability between the two states, we look at the 4.5- μm excesses, seen in Table 5, because Be stars, both classical and Herbig Ae/Be, are expected to show near-IR emission to some degree (see, e.g., Touhami et al. 2010). Indeed, we do see an excess ratio $> 3\sigma$ above the photospheric emission at 4.5 μm for 11 of the 16 OBe stars in our spectroscopic sample, as well as in 2 of the 7 “OBe?” stars. This could indicate that the other 10 OBe and “OBe?” stars were in a normal B-star phase during the IRAC observations, ac-

quired in 2005 May. These excesses, however, are weak, at less than 4 times the expected photospheric flux, suggesting that we may just be unable to detect the excesses in our remaining spectroscopically confirmed OBe stars because of the uncertainties ($\sim 20 - 30\%$) in their photospheric flux in our data. Adding further uncertainty is our use of J -band data to scale the photosphere, because Be stars may exhibit excesses even at wavelengths as short as $1.2 \mu\text{m}$. This can be seen in the slopes of the dashed lines in the SEDs of B 038, B 081, B 085, B 119, B 140, and B 190, for example, in Figures 9 and 10. The dashed lines are fit to $I - K$ and show shallower slopes than expected for the photospheric emission.

We also find 12 stars (B 023, B 033, B 047, B 115, B 128, B 135, B 136, B 142, B 154, B 156, B 160, and B 183) in Table 5 that do not show optical emission lines (see Table 4) but do have an excess ratio at $4.5 \mu\text{m}$ significant at the 3σ level. The $4.5\text{-}\mu\text{m}$ excesses are also weak, with only B 136 showing an excess/photospheric ratio greater than 1. This excess could indicate that these stars were in a Be state at the time of the IRAC photometry but settled into a normal B-star state by the time the spectra were acquired. If we assume that all of the $4.5\text{-}\mu\text{m}$ excesses are due to Be-star behavior, the fraction of transient Be-stars (counting as transient those OBe and “OBe?” optically classified stars without $4.5 \mu\text{m}$ excess, plus these 12 stars with $4.5 \mu\text{m}$ excess but no hint of $\text{H}\alpha$ emission in their spectra) is $22/47$, or about 47% of the total Be-star population in the sample. This is on par with the fraction seen in the study of Galactic Be-stars by McSwain et al. (2009). Therefore it seems unlikely that the remainder of our stars that show no Be activity in the photometry and spectra are primarily dormant Be-stars.

5.2. Herbig Ae/Be Stars

Because we do not know the ages of the Be stars in our sample, it is difficult to determine to which of the Be-star categories they belong. None of the Be stars we identified spectroscopically have the large excesses at $\lambda \gtrsim 1 \mu\text{m}$ that are typical of the hot dust in Herbig Ae/Be objects. Hillenbrand et al. (1992), however, identify in the Galaxy a set of objects with near-IR profiles that resemble classical Be stars, but are apparently young stars, located near reflection nebulae. This location is more typical of Herbig Ae/Be stars. Hillenbrand et al. (1993) suggest that these objects, which they label Group III, are actually Herbig Ae/Be stars that have an optically thin circumstellar disk, rather than the optically thick disk more typical of the Herbig Ae/Be class.

The weak $4.5\text{-}\mu\text{m}$ excesses of the Be stars detected in our spectroscopic study resemble the near-IR profiles of classical Be stars as well as these Group III objects. The stars in our sample are located within regions of recent star formation, suggesting an age of $\lesssim 10$ Myr. Unfortunately, 10 Myr is the approximate age at which classical Be stars begin to appear in clusters (Fabregat & Torrejón 2000), and so we cannot be certain whether these objects are young stars or older, established main-sequence stars without more accurate age determinations. The bulk of the dusty B-star sample, with neither optical emission lines nor a near-IR excess, are unlikely to be Herbig Ae/Be stars.

5.3. Cirrus Hot-Spots Comparison

Backman & Paresce (1993) note that to be certain that debris disks are the source of the excess infrared emission, spatially resolved observations of the disk are needed, because hot spots in the ISM can mimic the color temperatures and fractional luminosities of debris disks. The morphology of the dust is the best clue as to whether the heated dust is physically associated with the star in a disk, or if it is simply a concentration of ISM material close to the star. Unfortunately, at the distance of the SMC, debris disks cannot be resolved with any available facilities, and ISM hot spots are below the resolution of the *Spitzer* data, especially with a $6''$ resolution at $24 \mu\text{m}$.

Since we lack resolved images of the dust emission, we instead compare the dust properties of the SMC sample to the Galactic cirrus hot-spot sample of Gaustad & van Buren (1993). A broader comparison using *WISE* data is carried out in Paper II. The Gaustad & van Buren (1993) sample was selected by looking for *IRAS* excesses at $60 \mu\text{m}$ with color temperatures above the ~ 25 K temperature of the general Galactic cirrus and peaking at the location of a star, with $F_{\text{IR}}/F_{\text{Bol}} < 0.1$ to exclude H II regions, and spatially extended emission that is more extended in longer wavelengths, indicating that the temperature declines with distance from the star. We note that in cases where the reported *IRAS* $25\text{-}\mu\text{m}$ flux is negative, the color temperatures cannot be calculated.

Whether this cirrus hot-spot sample in fact consists solely of cirrus hot-spots is, however, uncertain. Gaustad & van Buren (1993) found that in some cases, the hot spots have $12\text{-}\mu\text{m}$ emission that is brighter than the $25\text{-}\mu\text{m}$ emission, indicating a hotter dust component than the expected ~ 70 K temperature of illuminated cirrus. Indeed, the color temperatures we find for the hot-spot sample from the 12/25 flux-ratios are all above 100 K. Furthermore, Kalas et al. (2002) used resolved optical images of nebulosity around three B stars that appear in both the Gaustad & van Buren (1993) and Backman & Paresce (1993) samples to model the IR emission from the objects. The authors concluded that, in all three cases, the ISM model cannot explain the 12- and $25\text{-}\mu\text{m}$ emission, requiring a source of warmer dust. The coronagraph used to block the starlight for their optical images unfortunately obscures the central 100–1000 au around the star, where a circumstellar disk would be located. The warmer dust could therefore be provided by a population of either blackbody grains in a close-in circumstellar disk, or very small grains at larger distances that are heated stochastically to higher temperatures than equilibrium. In cases where the stellar velocity is large compared to the local ISM (such as runaway stars), a bow-shock could further heat the dust in addition to stellar irradiation. Distinguishing between these scenarios would require imaging at higher resolution, which we discuss further in Paper II. The $12\text{-}\mu\text{m}$ *IRAS* band also contains a PAH emission feature, offering another possible explanation for the excess flux at that wavelength. Illustrating the difficulty of distinguishing disks from hot-spots using SED information alone, even for nearby objects, Kalas et al. (2002) note that 31 of the 34 B-type stars in the Backman & Paresce (1993) table of debris disk candidates or Vega-like stars, appear in the

Gaustad & van Buren (1993) cirrus hot-spot list.

The full hot-spot sample contains stars of spectral types O6 through B9 of all luminosity classes, but we exclude from the comparison any objects marked in the Gaustad & van Buren (1993) table as emission line stars or stars of luminosity class higher than V, to match the characteristics of the SMC dusty OB stars. We further limit the hot-spot sample to those objects that have excesses, if scaled to the SMC distance of 61.1 kpc, that we could detect at the $5\text{-}\sigma$ level or better at $24\text{ }\mu\text{m}$ in the S³MC survey (215 μJy ; Bolatto et al. 2007). This sub-sample contains 18 stars. We then calculated the dust parameters for this sub-set of the sample, using the $12/25\text{-}\mu\text{m}$ combination in place of $8/24\text{-}\mu\text{m}$, and these values are listed in Table 7. Stars flagged in Table 7 as “known reflection nebula” are noted in Gaustad & van Buren (1993) to have extended emission that is brighter in the blue than in the red on the Palomar Sky Survey or ESO Sky Survey plates.

The comparison SMC sample contains a total of 31 stars (c.f., Table 6), and it is constituted by normal main sequence stars (no OBe, “OBe?”, or Em classification) that have a measurable $8\text{ }\mu\text{m}$ emission excess, in order to determine the temperature of the dust. While the distributions in both samples over spectral types peak at a similar type – B0 in the SMC vs. B1 in the hot-spot sub-sample – the SMC sample extends more towards earlier types while the hot-spot sub-sample extends towards later types. This is reflected in the distributions over stellar effective temperature, shown in Figure 14.

In Figure 15 we show histograms of the observable parameters, F_8/F_{24} or F_{12}/F_{25} , L_{24} or L_{25} , and F_{24}/F_{Bol} or F_{25}/F_{Bol} . The IR luminosities and fractional IR luminosities are similar; the difference in the IR ratio is largely driven by the use of the 8- vs. $12\text{-}\mu\text{m}$ bands. In Figure 16 we show histograms of the color temperature, mass, and fractional luminosity, where the samples are restricted to spectral types O9–B2, since both samples have at least one star of each of these spectral types. The histograms for the hot spots in Figures 15 and 16 are created by weighting the number of objects in that sample so that the total number of hot spots in a spectral type bin equals the total number of objects in the bin for the SMC sample. In this manner the weighting controls for the different spectral makeup of the two samples. Figure 17 shows the averages of each of the observable parameters and associated dust parameters against stellar temperature, without the restrictions on visibility at the SMC distance that are used in the histograms.

The distributions over dust temperature are very similar for both samples. They both have similar mean temperatures in the 125–130 K range, although the hot-spot sample also displays a broader range in dust temperatures, 97–226 K compared to 116–164 K for the SMC sample. The hottest color temperatures in the hot-spot sample in Figure 15 result from the coolest and most predominant spectral type, B2. The trend toward higher color temperatures in the hot-spot sample is possibly due to PAH contamination. The $12\text{-}\mu\text{m}$ PAH emission feature remains relatively unchanged over a broad range of radiation field intensities, but the thermal emission at $25\text{ }\mu\text{m}$ changes dramatically (e.g., Figure 13 in Draine & Li 2007). Thus PAHs around cooler stars would create higher color temperatures than around hot-

ter stars; F_{12}/F_{25} would be artificially high as a result of similar amounts of PAH emission at $12\text{ }\mu\text{m}$ but reduced thermal emission at $25\text{ }\mu\text{m}$. This is likely a lesser effect in the SMC, where PAH emission is weak (e.g. Sandstrom et al. 2010).

The distributions over dust mass are also similar for both samples, though again the distribution appears broader (both towards higher and lower dust masses) in the hot-spot sample. The SMC sample may be devoid of examples of lower dust mass as these would not have been detected. The average mass at B0 and B1, where there is the greatest number of objects in both samples, is similar for each sample (Fig. 17), but the average dust mass in the SMC sample is higher at B2, and lower for O7–O9, compared to the cirrus hot-spots. We see a trend in the hot-spots of lower dust mass for cooler stars, which is reasonable given that a hotter, more massive star could illuminate larger regions of the ISM. We do not see this dependence on the stellar temperature for the SMC objects, although the smaller temperature range of the SMC sample would make such a trend perhaps difficult to detect.

At first glance, the distributions over F_{IR}/F_{Bol} do also appear similar between the two samples. On closer inspection, the one for the hot-spots is clearly broader. The average $F_{IR}/F_{Bol} = 4 \times 10^{-4}$ for the hot-spot sample is smaller than that of the SMC, which is $F_{IR}/F_{Bol} = 1.5 \times 10^{-3}$, although this is somewhat misleading as the averages are skewed by the extremes in the sample. The derived F_{IR}/F_{Bol} for both samples do fall within the typical 10^{-4} to 10^{-2} range of debris disks (Chen et al. 2006).

While we noted minor differences in the distributions over dust temperature, dust mass and F_{IR}/F_{Bol} between the SMC and hot-spots samples, these can be explained by a combination of small-number statistics, selection bias, and the opposite sense of skewedness of the distributions over spectral type. Indeed, Figure 17 shows that the trends – or absence thereof – and mean values are consistent between both samples if the breakdown over spectral types is taken into account.

Interestingly, despite the low dust-to-gas ratio in the SMC (about $1/7$ – $1/10$ that of the Milky Way; Leroy et al. 2007), the SMC objects show dust masses similar to the Galactic hot-spots if common selection thresholds are applied. This suggests that, if they are hot-spots, the mass of gas being illuminated is 7 – 10 times larger in the SMC than in the Milky Way. Assuming similar gas densities, this suggests that the typical sizes of hot-spots would be ~ 2 larger in the SMC than in the Milky Way.

5.4. Bow-shocks and Runaway Stars

Larger dust masses, warmer dust and thus brighter emission may arise from bow-shocks ahead of runaway stars, or stars being over-run by expanding interstellar bubbles. Stars with stronger stellar winds – i.e., of earlier type and/or at later evolutionary stages – and/or larger relative velocity with respect to the local ISM sweep up more mass; larger relative velocities also result in stronger shocks and hence greater heating. Gvaramadze et al. (2011) present a sample of 12 candidate runaway stars with bowshocks in the SMC.

Curiously, there is no overlap whatsoever between their sample and ours.

The distribution of our sample on the sky (Figure 18) seems to indicate that at least a portion of them are found outside of sites of vigorous star formation. While the late-B stars may be old enough to have migrated from their birth-sites or for their natal clouds to have dispersed, the fact that some of the O-type stars are also found outside star-forming regions suggests they may be runaways. One of our “normal” OB stars, B064 is in fact the primary in an X-ray binary², and it is likely that the binary system will have received a high peculiar velocity when the neutron star’s progenitor star exploded as a core-collapse supernova – see Kaper et al. (1997) for the proto-typical example of a bow-shock accompanied runaway X-ray binary, Vela X-1.

We also note that the structure of the ISM in the SMC differs in important ways from that in the Milky Way disk; the SMC is dominated by expanding bubbles (Staveley-Smith et al. 1997) while gas in the Milky Way disc is more strongly entrained and collected by the recurrence of a spiral density wave. This could affect the ubiquity and properties of bow-shocks; for instance stars in the SMC might be over-run by expanding shells (see Dawson et al. 2013, for such mechanisms operating within the Large Magellanic Cloud), resulting in large relative velocities between stars and ISM without the requirement for a “kick” velocity of the star.

While proper motions relative to the systemic motion of the SMC are too small to be measured ($1 \text{ mas yr}^{-1} \approx 300 \text{ km s}^{-1}$), radial velocities can be determined with much better accuracy. Our own spectroscopy, however, has neither the spectral resolving power nor velocity calibration accuracy required for such measurements. In Table 4 we list the radial velocities measured for stars in our sample by Evans et al. (2006), Martayan et al. (2007) and Evans & Howarth (2008). We also determined the velocity of the peak in the H I emission around the location of the star in question, from inspection of the datacube produced by Stanimirović et al. (1999). This differs from the intensity-weighted velocity map produced by Stanimirović et al. (2004), because we are interested in the most likely velocity difference between a star and the densest parts of the ISM. Often, more than one strong peak is seen in the H I data; in that case we list both. Of the 21 stars with radial velocity measurements, most stellar kinematics coincide with that of a strong H I peak. B116, B124 (and perhaps B119) fall in between H I peaks, suggesting they might reside in the middle of a shell expanding at $\sim 18\text{--}20 \text{ km s}^{-1}$. But two O7 stars, B142 and especially B145, have large velocity differences of ~ 35 and 75 km s^{-1} with respect to the nearest (in velocity) H I peak. No uncertainties were quoted for the stellar radial velocities for these stars, but measurements for other stars from the same work (with the caveat that those were all later spectral type) often agreed with H I kinematics, which suggests typical errors not much larger than $\sim 10 \text{ km s}^{-1}$. We thus suggest that these two O7 stars may be runaways – they are located just outside of the brightest H II region in the SMC, LHA 115-N66 containing the massive O-star cluster NGC 346, lending

further support to their large space velocities.

5.5. Disks

Statistics for circumstellar disk detections around stars with spectral types as early as the SMC sample are difficult to come by. Few surveys exist of stars younger than 10 Myr, which encompasses most, if not all, of the main-sequence lifetimes of these late-O and early-B stars, and those surveys that do sample the appropriate age range still contain very few stars of these types (see Carpenter et al. 2009, and references therein).

Our sample of 87 objects with normal O- or B-star main sequence spectra in the SMC shows excesses at $24 \mu\text{m}$ that are larger than those of typical debris disks, in studies of somewhat less massive (late-B and A-type) stars in the Milky Way. Carpenter et al. (2009) set a limit, based on the properties of their sample of B7–A9 stars, for the ratio of observed flux to expected photospheric flux at $24 \mu\text{m}$ of $\lesssim 100$ for debris disks (but only a ratio of $\lesssim 5$ for solar-type stars). Any object with a larger ratio is considered to be a primordial disk. Hernández et al. (2006) define objects with $K - [24] \gtrsim 5$ mag as Herbig Ae/Be stars, while objects below this limit are debris disks. Hernández et al. (2006) also define any object with $2.3 \lesssim K - [24] \lesssim 5$ mag as a massive debris disk. The SMC objects have observed flux to expected photospheric ratios $\gtrsim 70$, with only 6 objects being less than 100 and a further 7 objects being within 1σ of 100. The SMC objects also have $K - [24] \gtrsim 3.4$ mag, with only 11 objects below the limit of 5. Of those 11, we identify 7 as OBe stars.

The studies of Hernández et al. (2006) and Carpenter et al. (2009) only consider circumstellar matter around intermediate and low mass stars, so it is possible that these dividing limits around the more massive stars in our SMC sample should be higher. Carpenter et al. (2009), however, specifically excluded earlier type stars from consideration because, aside from being few in number, they may show a severely reduced dust luminosity due to the loss of small grains to radiation pressure. We find blowout grain sizes for the SMC objects on the order of 1 mm, in the absence of gas drag (see Table 6). The smallest dust grains are the most efficient (per unit mass) at capturing and reprocessing UV and optical radiation into infrared. This suggests that, if blowout is significant, F_{IR}/F_{Bol} started much larger than we currently measure in our sample.

Hernández et al. (2006) suggest two scenarios to explain massive circumstellar dust disks. They could be the result of collisions between two large planetesimals, greater than 1000 km, or they could be explained as a transition phase from Herbig Ae/Be star to debris disks, in which the disk still contains a significant fraction of primordial dust. The small number of these objects detected in the SMC sample suggests that they could be in a short-lived phase, and perhaps constitute transition disks remnants from the stellar accretion. In the original S³MC sample, the $24\text{-}\mu\text{m}$ excess objects were 5% of the total number of objects that met the requirements for normal late-O and early-B stars in the specific magnitude and color cuts (Bolatto et al. 2007). Counting only the stars that have normal O- and B-star spectra, which is 87 out of the 193 objects in the original list, and also

² The other primary in an X-ray binary in our sample, B085, is a Be star and therefore excluded here from further analysis

assuming that all of these objects are debris disks, rather than ISM hot spots or quiescent Be stars, gives a detection fraction of only 2.2%. Including the 45 objects for which we have no spectra to judge their emission-line star status gives a maximum of 3.4%. If the possible transition object that Hernández et al. (2006) detect is truly in this transition phase, that would give a detection fraction of 3% for transition objects in the 5 Myr cluster in which it lies. This detection fraction is consistent with that seen in the SMC sample.

Finally, it is worth noting that comparison with literature classifications shows that a significant fraction of our SMC sample consists of binaries. The effect of binary systems on the formation of circumstellar disks is unclear. One might expect the disks to be dynamically disrupted, although circumbinary planets have been recently discovered by *Kepler* (Doyle et al. 2011; Welsh et al. 2012; Orosz et al. 2012a,b; Schwamb et al. 2012).

6. SUMMARY AND CONCLUSIONS

We obtained long-slit spectra of 125 of the 193 dusty OB stars in the S³MC survey that show large excess emission at 24 μ m. These new observations cover a significant fraction of the sample, make possible accurate sky removal in the complex regions where these stars live, and allow us to draw robust conclusions on the statistics of different contributors to the sample.

We use these spectra to classify the stars and look for the signatures of the OBe activity. We find 87 objects that lack emission lines and appear to be normal, main sequence late-O/early-B main-sequence stars. For these stars, we use our spectral classification to estimate their luminosity, and calculate the dust temperature, dust mass, F_{IR}/F_{Bol} , and equilibrium dust distance from the host star. We discuss the spectral and photometric properties of our sample in relation to several possible scenarios: classical Be stars, massive analogs of Herbig Ae/Be stars, hot-spots in the interstellar medium (possibly with contributions of bow-shocks), and disks. The results of this study are:

- We identify 17 stars in the dusty O and B stars sample as OBe stars because of clear H α emission in their spectra (this count includes B094, the object with forbidden nitrogen emission). A further 7 stars exhibit weaker than expected H α absorption and are therefore classified as possible OBe stars – one of these is an O6Iaf star showing He II 4686 Å emission. We also identify 12 stars that show no H α emission in their spectra but do show 4.5 μ m excess in the photometry that could be indicative of transient Be-star activity. If these 12 stars are dormant OBe stars, along with the 11 spectroscopically identified OBe stars that show no excess at 4.5 μ m, the transient total OBe star fraction would be $\sim 47\%$. This fraction is consistent with the study of transient Be star activity by McSwain et al. (2009). Thus it seems unlikely

that the remaining 75 stars, with neither 4.5 μ m excesses nor H α emission, are OBe stars that happened to be in normal OB star states during both the photometric and spectroscopic observations.

- Our dusty OB stars are generally located near regions of recent star formation, similar to Herbig Ae/Be type stars, and in that respect resemble the Group III Herbig Ae/Be objects in Hillenbrand et al. (1992). Our objects have ages $\lesssim 10$ Myr. Note that classical Be-star activity begins to appear in clusters around 10 Myr of age, once again suggesting that the majority of them cannot be explained by excretion disks with a dusty component.
- The SMC sample exhibits broadly similar characteristics when compared to the cirrus hot-spot sample of Gaustad & van Buren (1993). The hot-spot sample shows trends for decreasing dust temperature and increasing dust mass for hotter stars, which the SMC sample does not. However, these differences likely arise from the different distributions over spectral type, and perhaps stronger contamination of the broadband colors by PAHs in the Milky Way. We show evidence that at least some of the stars in the SMC sample are runaways, including one X-ray binary; heating in a bow-shock could add to the radiative heating of the dust.
- The SMC sample of objects show higher 24 μ m excesses than typical debris disks around intermediate mass stars in the Milky Way. There are not enough debris disks known around comparably massive stars, however, to indicate what is typical for an early-B or late-O debris disk. Alternatively, if the stars are young, we may be observing the remnants of the accretion process — analogs to transition disks around massive stars. The detection fraction of these objects when compared to stars with similar optical colors and luminosities is 2.2%–3.5%, which is consistent with the expected short lifetime of a transition phase.

We analyze and discuss additional observations of the SMC dusty OB sample, as well as further comparison with a sample of massive stars in the Galaxy compiled using *WISE* photometry, in Paper II.

Based on observations obtained at the European Southern Observatory, programme 079.C-0485 (PI J.Th.van Loon). A. D. B. wishes to acknowledge partial support from a CAREER grant NSF-AST0955836, JPL-1433884, and from a Research Corporation for Science Advancement Cottrell Scholar award. This research has made use of the SIMBAD database, operated at CDS, Strasbourg, France. A. D. B. thanks Paul Kalas and Eugene Chiang for discussions that spurred the initial stages of this research.

REFERENCES

- Adams, J. J., Simon, J. D., Bolatto, A. D., Sloan, G. C., Sandstrom, K. M., Schmiedeke, A., van Loon, J. Th., Oliveira, J. M., & Keller, L. D. 2013, ApJsubmitted (Paper II)
- Allen, C. W. 1973, London: University of London, Athlone Press
- Alexander, R. D., Clarke, C. J., & Pringle, J. E. 2006, MNRAS, 369, 229

- Aller, L. H., et al. 1982, Landolt-Bornstein: Numerical Data and Functional Relationships in Science and Technology
- André, P., Men'shchikov, A., Bontemps, S., et al. 2010, *A&A*, 518, L102
- Antoniu, V., Hatzidimitriou, D., Zezas, A., & Reig, P. 2009, *ApJ*, 707, 1080
- Arny, T. 1977, *ApJ*, 217, 83
- Backman, D. E., & Paresce, F. 1993, *Protostars and Planets III*, 1253
- Bolatto, A. D., et al. 2007, *ApJ*, 655, 212
- Bonanos, A. Z., et al. 2010, *AJ*, 140, 416
- Burns, J. A., Lamy, P. L., & Soter, S. 1979, *Icarus*, 40, 1
- Carpenter, J. M., Mamajek, E. E., Hillenbrand, L. A., & Meyer, M. R. 2009, *ApJ*, 705, 1646
- Castelli, F., & Kurucz, R. L. 2003, *Modelling of Stellar Atmospheres*, 210, 20P
- Cesaroni, R., Galli, D., Lodato, G., Walmsley, C. M., & Zhang, Q. 2007, *Protostars and Planets V*, 197
- Chen, C. H., et al. 2006, *ApJS*, 166, 351
- Cieza, L. A., Schreiber, M. R., Romero, G. A., et al. 2010, *ApJ*, 712, 925
- Coe, M. J., et al. 2011, *MNRAS*, 414, 3281
- Dawson, J. R., McClure-Griffiths, N. M., Wong, T., Dickey, J. M., Hughes, A., Fukui, Y., & Kawamura, A. 2013, *ApJ*, 763, 56
- Dekker, H., Delabre, B., & Dodorico, S. 1986, *Proc. SPIE*, 627, 339
- Doyle, L. R., Carter, J. A., Fabrycky, D. C., et al. 2011, *Science*, 333, 1602
- Draine, B. T., & Lee, H. M. 1984, *ApJ*, 285, 89
- Draine, B. T., & Li, A. 2007, *ApJ*, 657, 810
- Evans, C. J., Howarth, I. D., Irwin, M. J., Burnley, A. W., & Harries, T. J. 2004, *MNRAS*, 353, 601
- Evans, C. J., Lennon, D. J., Smartt, S. J., & Trundle, C. 2006, *A&A*, 456, 623
- Evans, C. J., & Howarth, I. D. 2008, *MNRAS*, 386, 826
- Fabregat, J., & Torrejón, J. M. 2000, *A&A*, 357, 451
- Fazio, G. G., et al. 2004, *ApJS*, 154, 10
- Flower, P. J. 1996, *ApJ*, 469, 355
- Gaustad, J. E., & van Buren, D. 1993, *PASP*, 105, 1127
- Gordon, K. D., et al. 2011, *AJ*, 142, 102
- Gvaramadze, V. V., Pflamm-Altenburg, J., & Kroupa, P. 2011, *A&A*, 525A, 17
- Herbig, G. H., & Simon, T. 2001, *AJ*, 121, 3138
- Hernández, J., Briceño, C., Calvet, N., Hartmann, L., Muzerolle, J., & Quintero, A. 2006, *ApJ*, 652, 472
- Hildebrand, R. H. 1983, *QJRAS*, 24, 267
- Hillenbrand, L. A., Massey, P., Strom, S. E., & Merrill, K. M. 1993, *AJ*, 106, 1906
- Hillenbrand, L. A., Strom, S. E., Vrba, F. J., & Keene, J. 1992, *ApJ*, 397, 613
- Hunter, I., Lennon, D. J., Dufton, P. L., Trundle, C., Simón-Díaz, S., Smartt, S. J., Ryans, R. S. I., & Evans, C. J. 2008, *A&A*, 479, 541
- Ita, Y., et al. 2010, *PASJ*, 62, 273
- Kalas, P., Graham, J. R., Beckwith, S. V. W., Jewitt, D. C., & Lloyd, J. P. 2002, *ApJ*, 567, 999
- Kaper, L., van Loon, J. Th., Augusteijn, T., Goudfrooij, P., Patat, F., Waters, L. B. F. M., & Zijlstra, A. A. 1997, *ApJ*, 475, L37
- Keller, S. C., & Wood, P. R. 2006, *ApJ*, 642, 834
- Krivov, A. V. 2010, *Research in Astronomy and Astrophysics*, 10, 383
- Leroy, A., Bolatto, A., Stanimirović, S., Mizuno, N., Israel, F., & Bot, C. 2007, *ApJ*, 658, 1027
- Martayan, C., Frémat, Y., Hubert, A.-M., Floquet, M., Zorec, J., & Neiner, C. 2007, *A&A*, 462, 683
- Martínez-Galarza, J. R., Kamp, I., Su, K. Y. L., Gáspár, A., Rieke, G., & Mamajek, E. E. 2009, *ApJ*, 694, 165
- Martins, F., Schaerer, D., & Hillier, D. J. 2005, *A&A*, 436, 1049
- Massey, P., Puls, J., Pauldrach, A. W. A., Bresolin, F., Kudritzki, R. P., & Snow, T. 2005, *ApJ*, 627, 477
- McSwain, M. V., Huang, W., & Gies, D. R. 2009, *ApJ*, 700, 1216
- Meyssonnier, N., & Azzopardi, M. 1993, *A&AS*, 102, 451
- Miroshnichenko, A. S., & Bjorkman, K. S. 2000, *IAU Colloq.* 175: The Be Phenomenon in Early-Type Stars, 214, 484
- Nieva, M. F. 2013, *A&A*, 550, A26
- Oliveira, J. M., et al. 2013, *MNRAS*, 428, 3001
- Orosz, J. A., Welsh, W. F., Carter, J. A., et al. 2012, *ApJ*, 758, 87
- Orosz, J. A., Welsh, W. F., Carter, J. A., et al. 2012, *Science*, 337, 1511
- Ostlie, D. A., & Carroll, B. W. 1996, *An Introduction to Modern Stellar Astrophysics*
- Pagel, B. E. J., Edmunds, M. G., Fosbury, R. A. E., & Webster, B. L. 1978, *MNRAS*, 184, 569
- Planck Collaboration, Abergel, A., Ade, P. A. R., et al. 2011, *A&A*, 536, A24
- Porter, J. M., & Rivinius, T. 2003, *PASP*, 115, 1153
- Rieke, G. H., & Lebofsky, M. J. 1985, *ApJ*, 288, 618
- Rieke, G. H., et al. 2004, *ApJS*, 154, 25
- Sana, H., de Koter, A., de Mink, S. E., et al. 2013, *A&A*, 550, A107
- Sana, H., de Mink, S. E., de Koter, A., et al. 2012, *Science*, 337, 444
- Sandstrom, K. M., Bolatto, A. D., Draine, B. T., Bot, C., & Stanimirović, S. 2010, *ApJ*, 715, 701
- Schlegel, D. J., Finkbeiner, D. P., & Davis, M. 1998, *ApJ*, 500, 525
- Schwamb, M. E., Orosz, J. A., Carter, J. A., et al. 2012, *arXiv:1210.3612*
- Silaj, J., Jones, C. E., Tycner, C., Sigut, T. A. A., & Smith, A. D. 2010, *ApJS*, 187, 228
- Skrutskie, M. F., et al. 2006, *AJ*, 131, 1163
- Sloan, G. C., et al. 2004, *ApJ*, 614, L77
- Smith, R., & Wyatt, M. C. 2010, *A&A*, 515A, 95
- Sota, A., Maíz-Apellániz, J., Walborn, N. R., Alfaro, E. J., Barbá, R. H., Morrell, N. I., Gamen, R. C., Arias, & J. I. 2011, *ApJS*, 193, 24
- Stanimirović, S., Staveley-Smith, L., Dickey, J. M., Sault, R. J., & Snowden, S. L. 1999, *MNRAS*, 302, 417
- Stanimirović, S., Staveley-Smith, L., & Jones, P. A. 2004, *ApJ*, 604, 176
- Staveley-Smith, L., Sault, R. J., Hatzidimitriou, D., Kesteven, M. J., & McConnell, D. 1997, *MNRAS*, 289, 225
- Su, K. Y. L., et al. 2006, *ApJ*, 653, 675
- Takeuchi, T., & Artymowicz, P. 2001, *ApJ*, 557, 990
- Terebey, S., & Fich, M. 1986, *ApJ*, 309, L73
- Testor, G. 2001, *A&A*, 372, 667
- Touhami, Y., et al. 2010, *PASP*, 122, 379
- Udalski, A., Szymański, M., Kubiak, M., Pietrzyński, G., Woźniak, P., & Żebruń, K. 1998, *Acta Astronomica*, 48, 147
- van Buren, D., & McCray, R. 1988, *ApJ*, 329, L93
- van Loon, J. Th., Oliveira, J. M., Gordon, K. D., Sloan, G. C., & Engelbracht, C. W. 2010, *AJ*, 139, 1553
- Waters, L. B. F. M., & Marlborough, J. M. 1994, *IAU Symposium 162: Pulsation; rotation; and mass loss in early-type stars (Kluwer)*, 399
- Waters, L. B. F. M., & Waelkens, C. 1998, *ARA&A*, 36, 233
- Welsh, W. F., Orosz, J. A., Carter, J. A., et al. 2012, *Nature*, 481, 475
- Werner, M. W., et al. 2004, *ApJS*, 154, 1
- White, R. E., & Bally, J. 1993, *ApJ*, 409, 234
- Zaritsky, D., Harris, J., Thompson, I. B., Grebel, E. K., & Massey, P. 2002, *AJ*, 123, 855

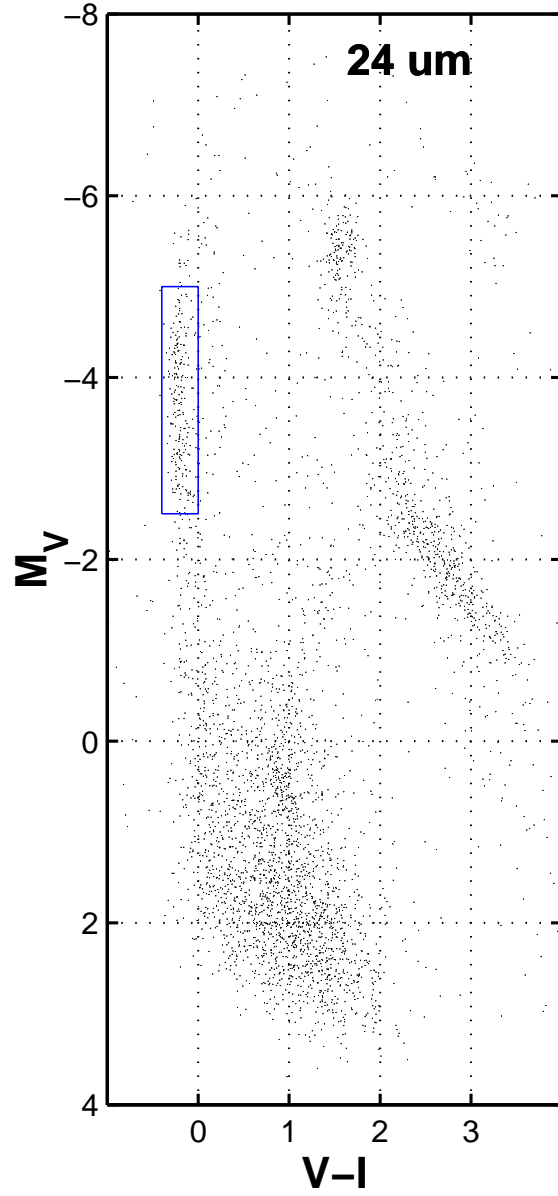


FIG. 1.— $V, V - I$ color-magnitude diagram for all of the stars detected at $24\ \mu\text{m}$ in the S³MC survey. The box indicates the objects with M_V and $V - I$ consistent with main-sequence late-O and early-B stars ($-5 < M_V < -2.5$ mag and $-0.4 < V - I < 0$ mag). The photospheres of such stars should not be detectable at $24\ \mu\text{m}$ in the S³MC survey.

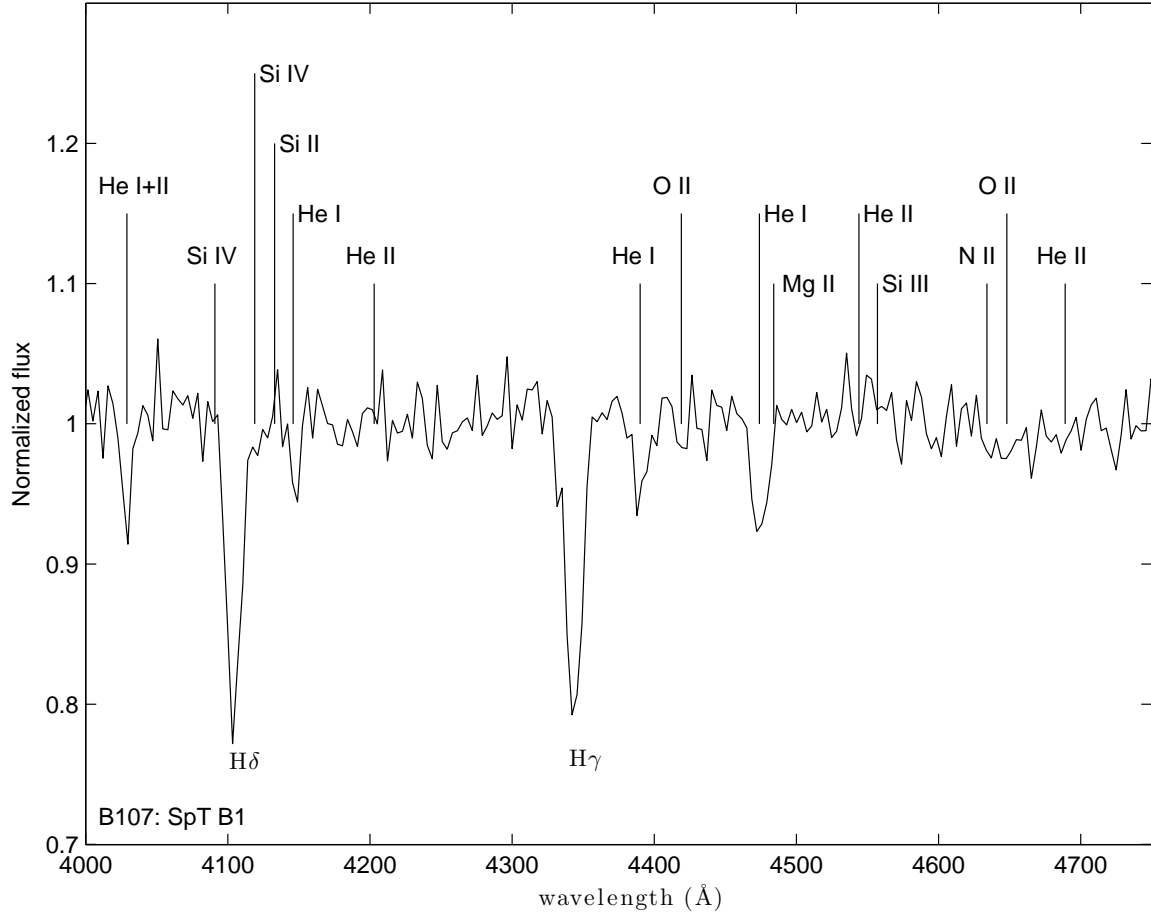


FIG. 2.— Example optical spectrum of one of the SMC dusty OB stars, B107. To demonstrate the classification system, the important lines are marked. The lack of He II lines indicates that it is a B star, and the lack of Si III lines suggests it is not a B2/B3 star. The Mg II line, however, is too weak for a star later than B3, so we conclude that the star is a B1, with the Si IV lines blended with H δ .

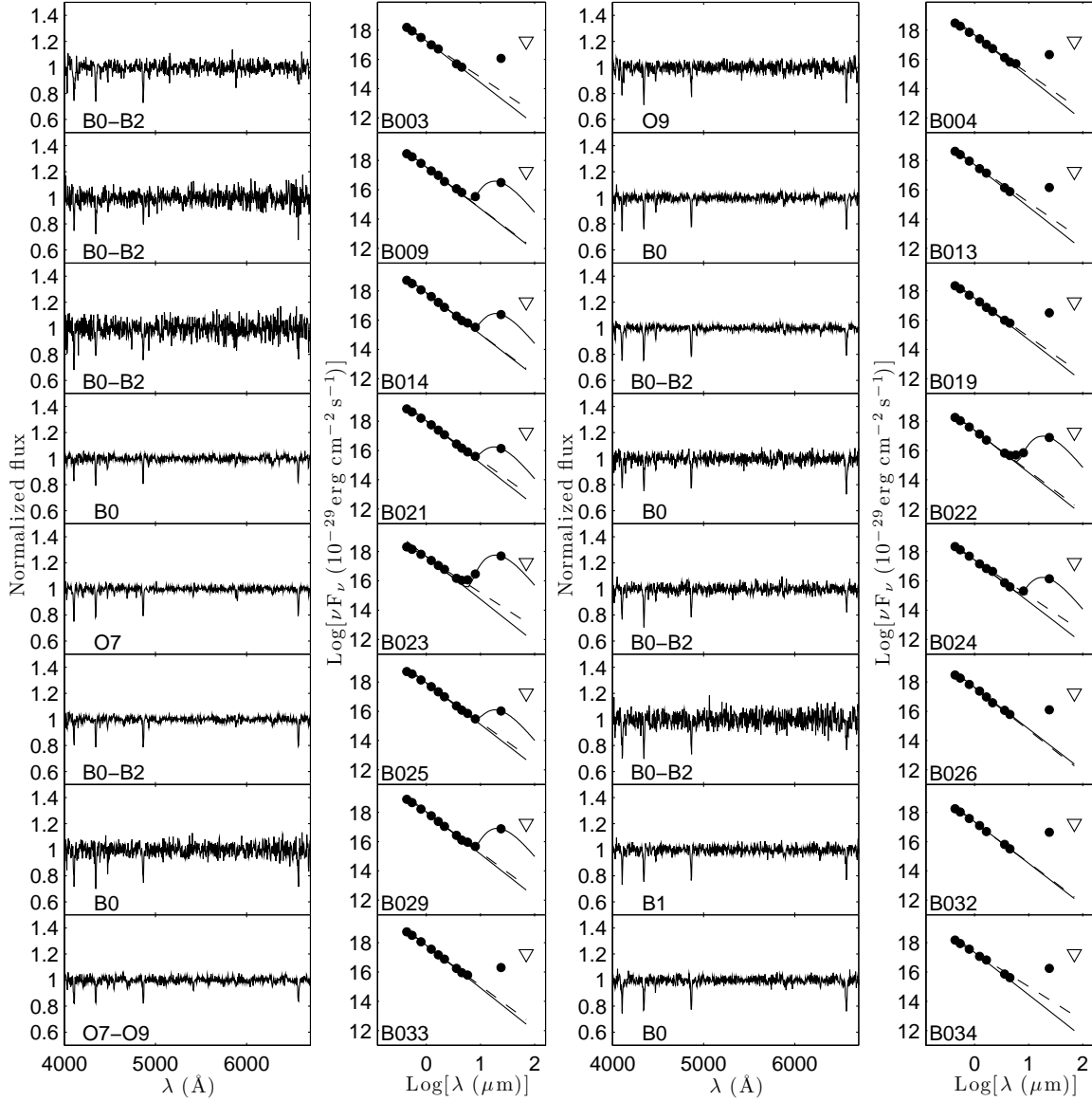


FIG. 3.— Spectra and SEDs of the objects with spectra of normal late-O and early-B stars. The solid line represents the fit of Equation 1 to the data using the slope from the spectral type, scaled by the J flux, or I if J was unavailable. Stars with a type O7–O9 use a slope of -2.91 , which is the slope for all stars in that range, while stars with type B0–B2 use a slope corresponding to B1. The dashed line is a fit of Equation 1 to the $I-K$ points, when available, without a fixed slope. Also plotted as a solid line is the total emission from the dust plus the photosphere, in cases where the $8/24\ \mu\text{m}$ color temperature was determined. The open triangle indicates the flux limit at $70\ \mu\text{m}$, and, for the few objects with a $70\ \mu\text{m}$ detection, the total dust plus photosphere emission for the $24/70\ \mu\text{m}$ dust temperature is also plotted. Important lines are those marked in Figure 2, as well as $\text{H}\alpha$ at $6563\ \text{\AA}$, $\text{H}\beta$ at $4861\ \text{\AA}$, and $\text{He I } 5876\ \text{\AA}$. The $[\text{O III}] 5007\ \text{\AA}$ line was used to gauge the effectiveness of the subtraction of the background H II region. The $B-H$ fluxes have been corrected for the foreground extinction by the Milky Way.

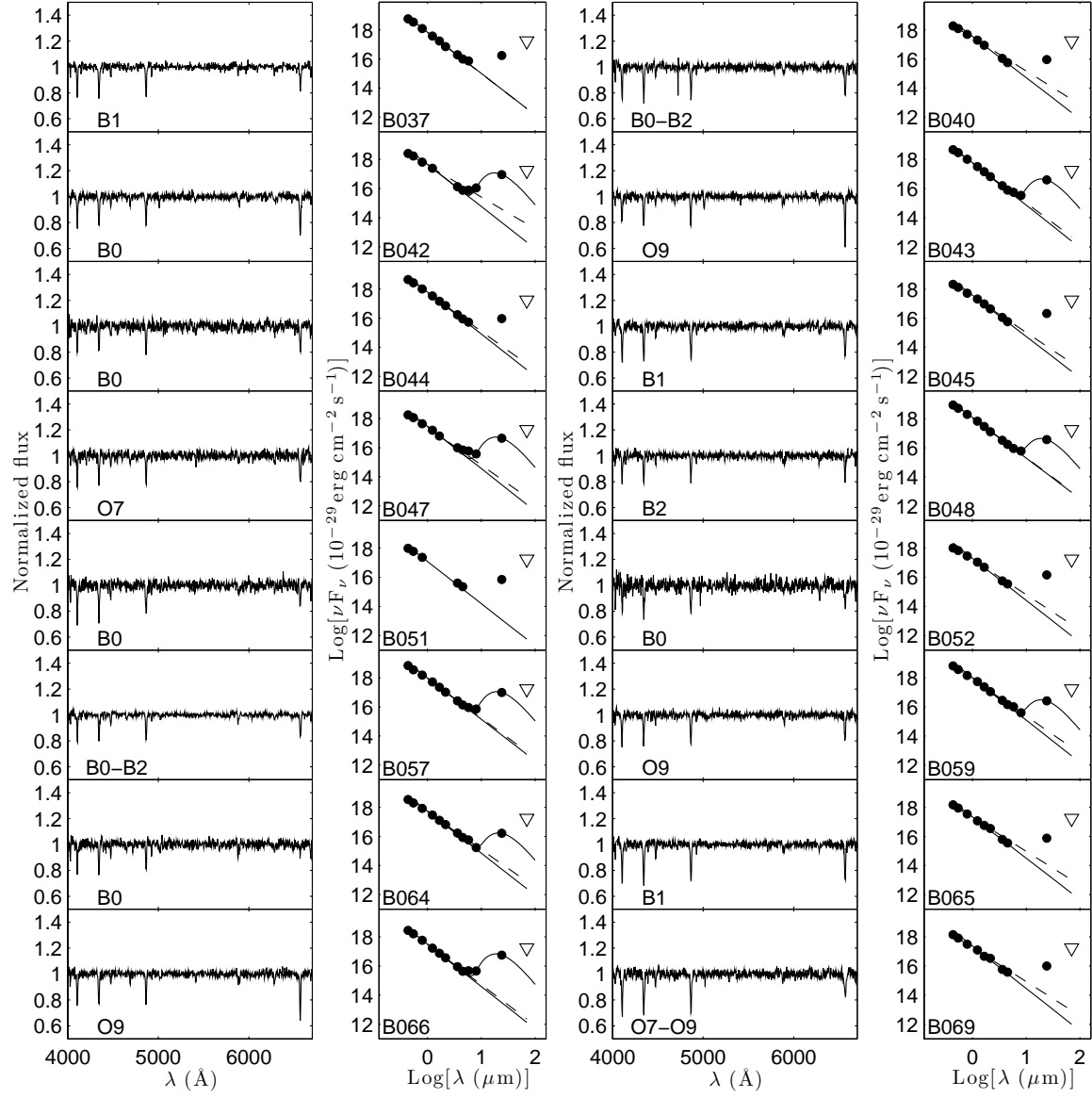


FIG. 4.— Same as Figure 3.

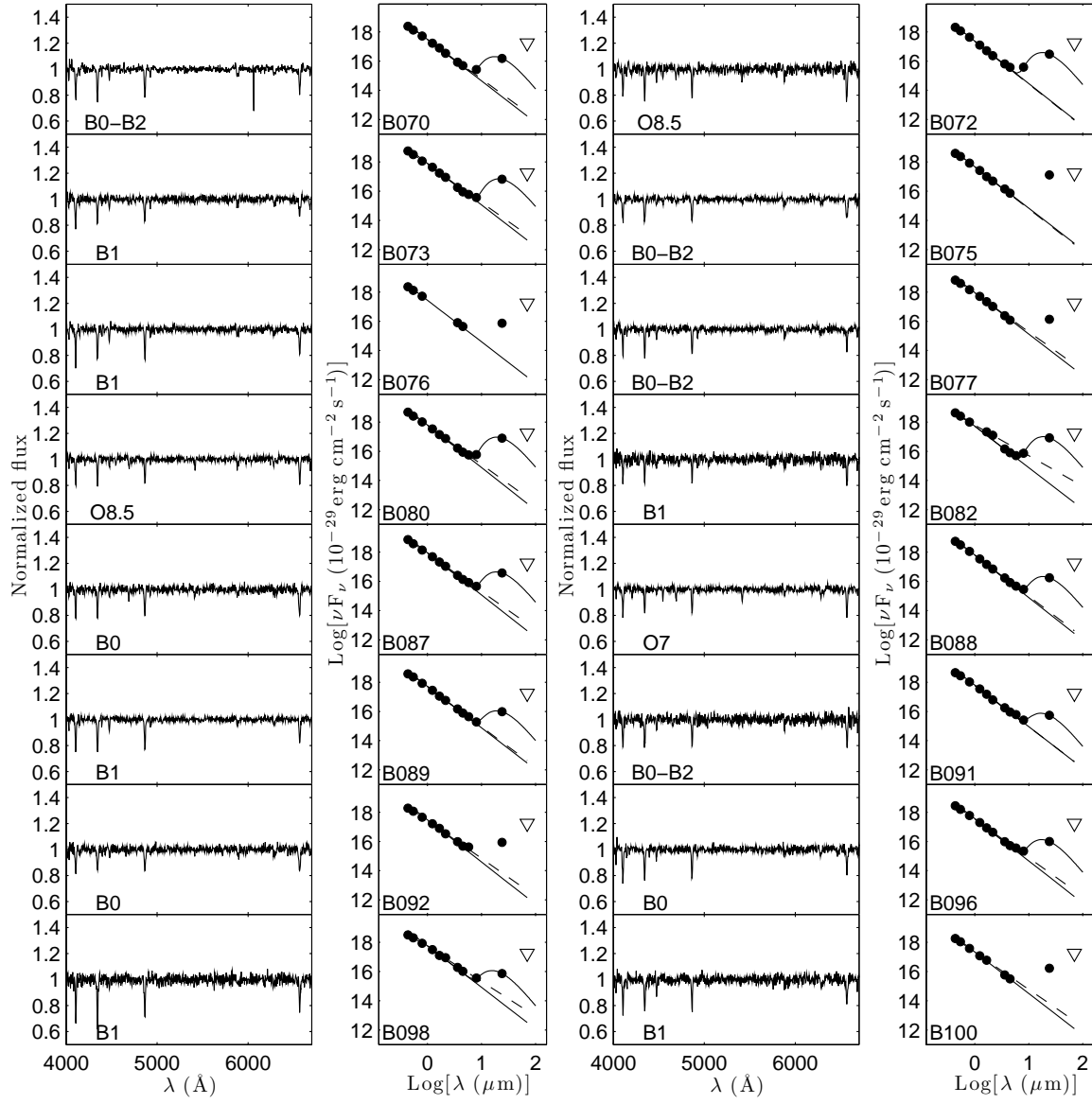


FIG. 5.— Same as Figure 3.

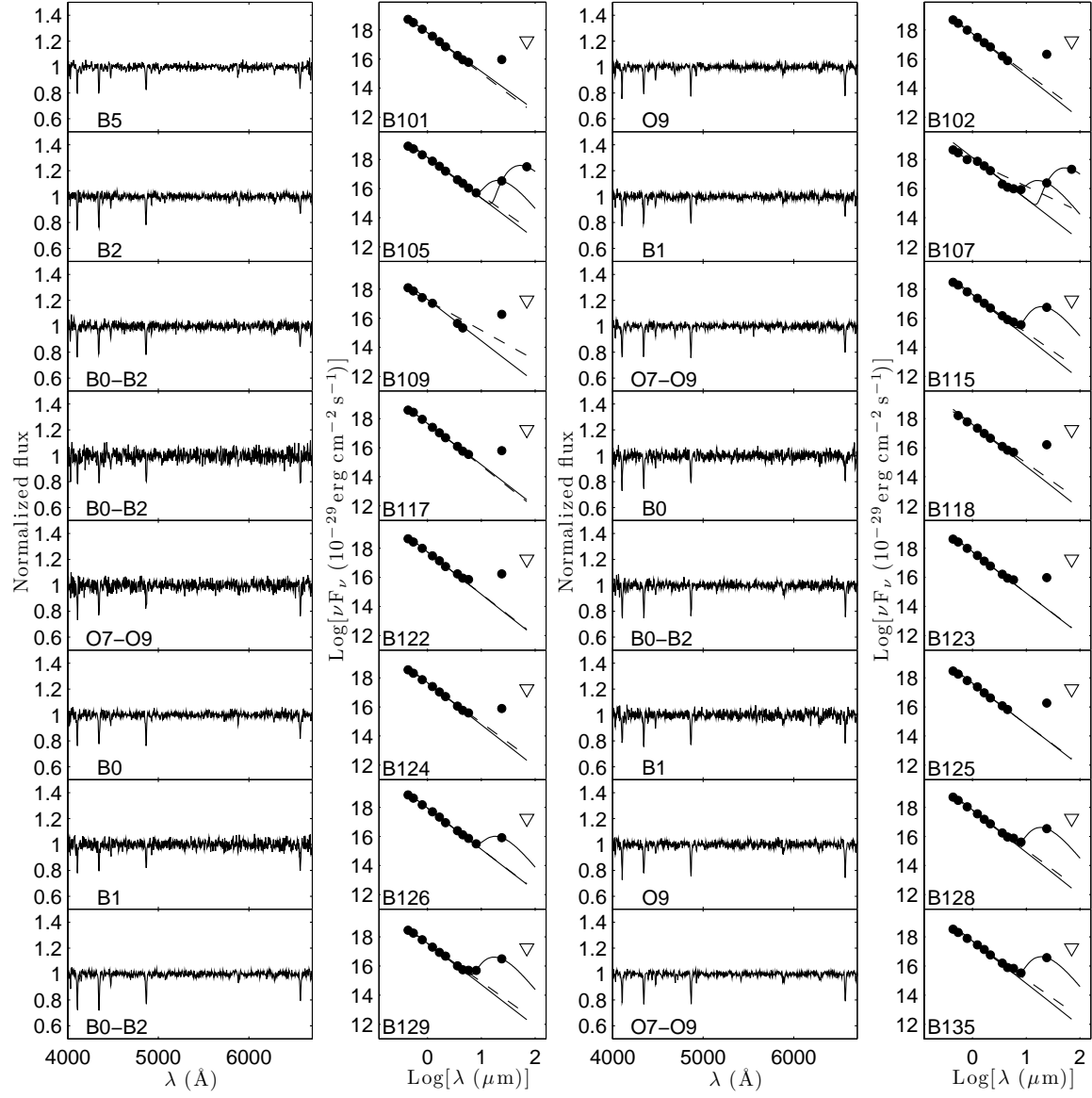


FIG. 6.— Same as Figure 3.

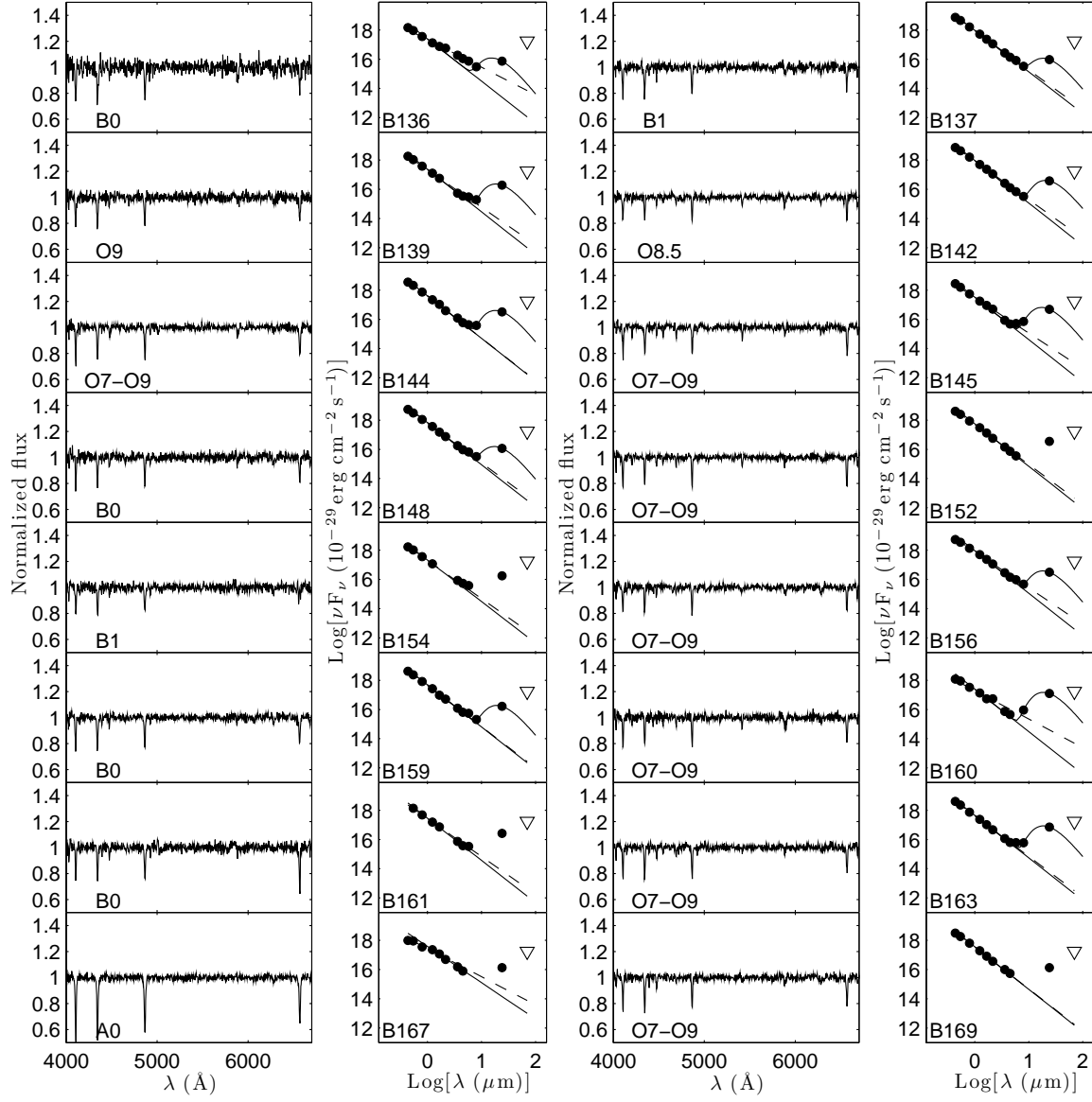


FIG. 7.— Same as Figure 3.

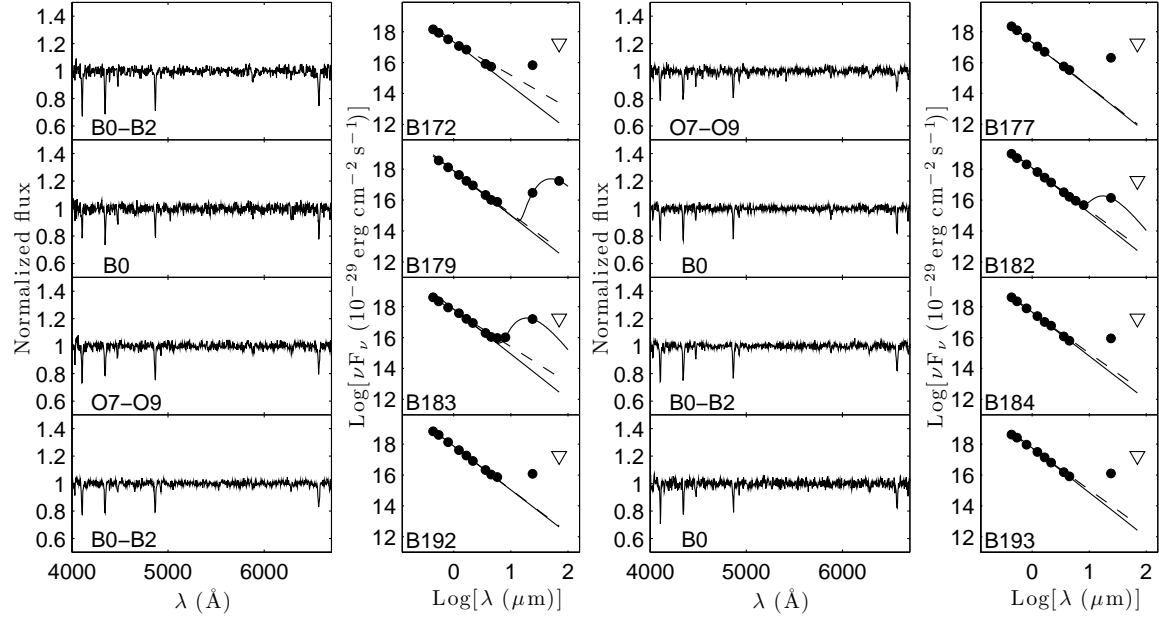


FIG. 8.— Same as Figure 3.

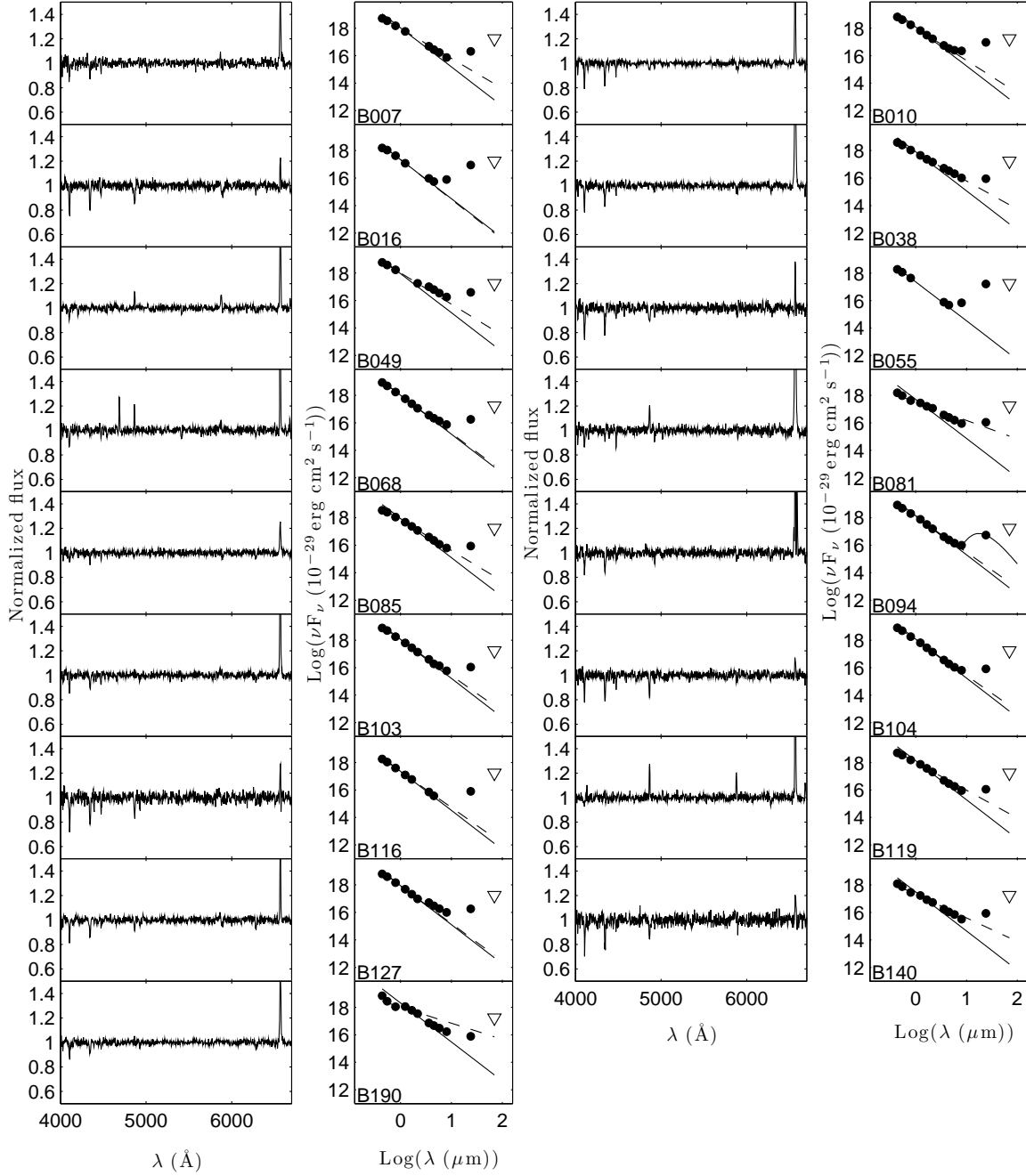


FIG. 9.— Spectra and SEDs, as in Figure 3, of the objects that we identify as Be stars based on the Balmer emission with no [O III] 5007 Å emission, a line whose absence we take to indicate that background subtraction is complete. The slopes of the solid lines in the SEDs correspond to a spectral type of B1, because the potential for He I/II emission makes Be stars difficult to classify. B 094 is unusual in that it shows [N II] emission, but no [O III]. We place it in the Be-star group because the H α emission, with the rest of the Balmer series in absorption, more closely resembles the Be stars than the group with strong Balmer and [O III] emission.

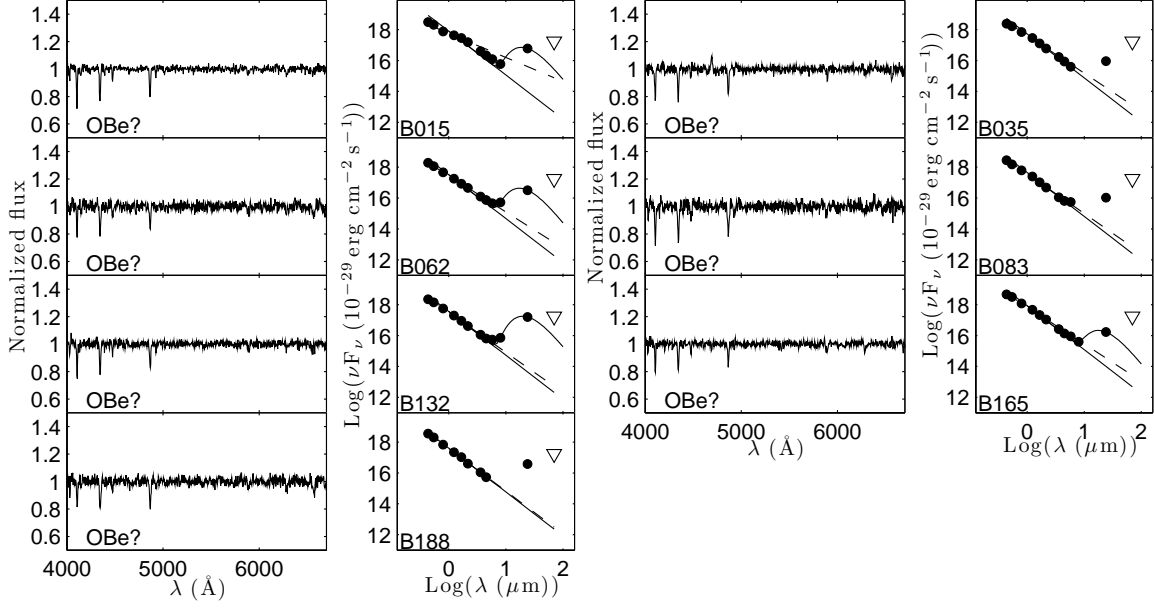


FIG. 10.— Spectra and SEDs, as in Figure 3, of the objects that show unusually little absorption at $H\alpha$ and are potentially Be stars whose photospheric $H\alpha$ absorption has not been filled in completely by the emission of the circumstellar matter. The slopes of the solid lines in the SEDs are set as in Figure 9.

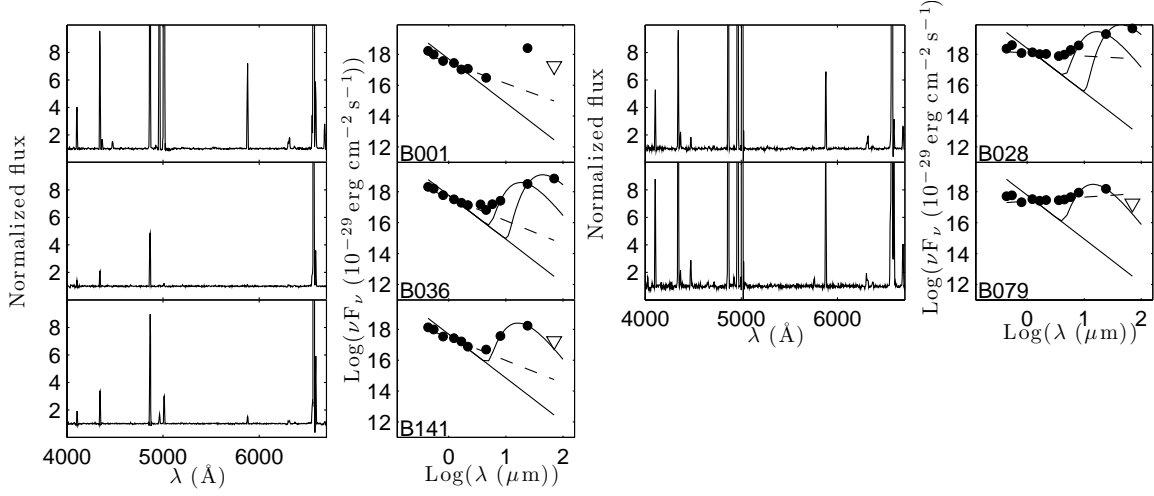


FIG. 11.— Spectra and SEDs, as in Figure 3, of the forbidden-line emission objects. The slopes of the solid lines in the SEDs correspond to a spectral type of B1. B 001, B 028, B 079, and B 141 are believed to be compact H II regions, given the strength of the forbidden emission, while B 036 has been identified as a young stellar object (Oliveira et al. 2013).

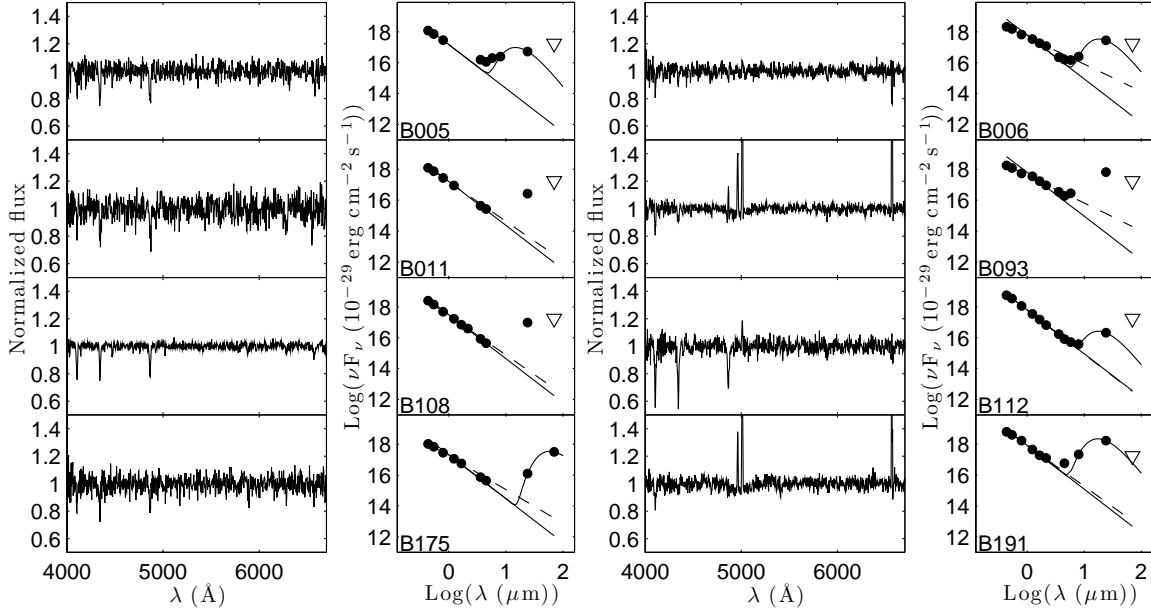


FIG. 12.— Spectra and SEDs of the objects for which background subtraction was difficult. B 005, B 011, B 112, and B 175 all suffer from low signal-to-noise due to clouds, and, except for B 011, they all have other objects nearby on the slit. B 006, B 093, B 108, and B 191 are embedded in a complex region of H α emission, making it difficult to determine the appropriate background level to subtract from the stellar spectrum. The slopes of the solid lines in the SEDs again correspond to a type of B1, given the lack of a classification.

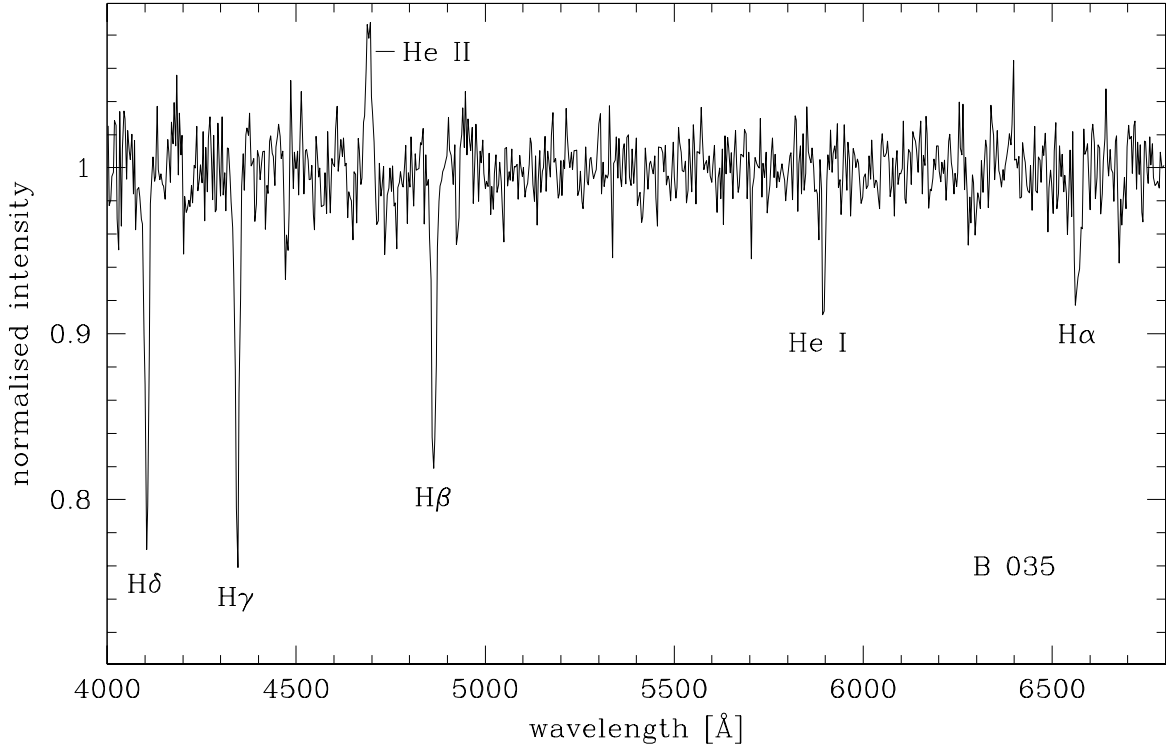


FIG. 13.— Spectrum of B 035, which exhibits He II 4686 Å emission indicative of an Ia supergiant luminosity class. The relative strength of the He I and He II lines suggests a spectral type around O6; the N III 4640 Å complex is weak, possibly due to the low metallicity of the SMC.

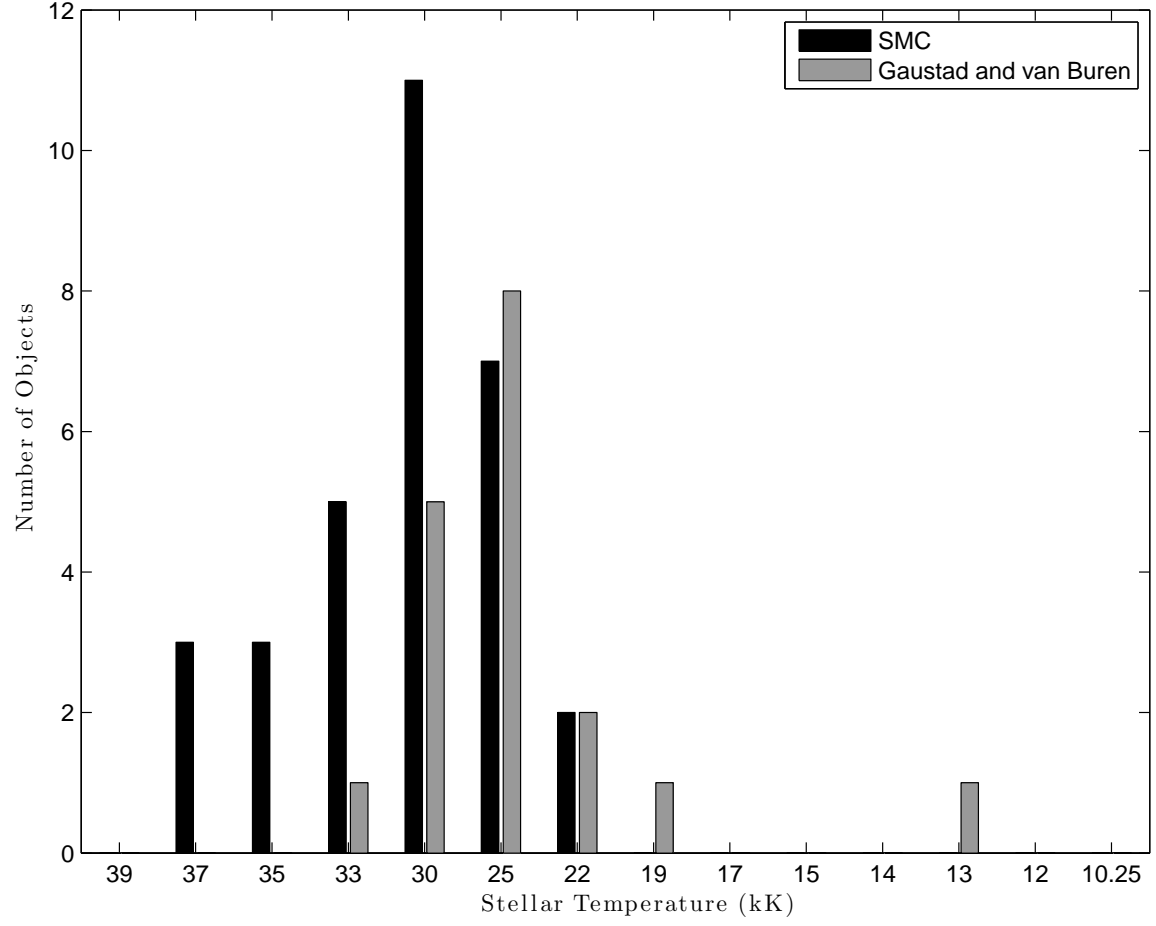


FIG. 14.— Total number of objects in each stellar temperature bin for which the 8/24 or 12/25 dust temperature has been calculated in Tables 6 and 7. The SMC sample is shown in black, while the Gaustad & van Buren (1993) sample of Galactic cirrus hot-spots is shown in gray. There are 31 SMC stars and 18 hot spots.

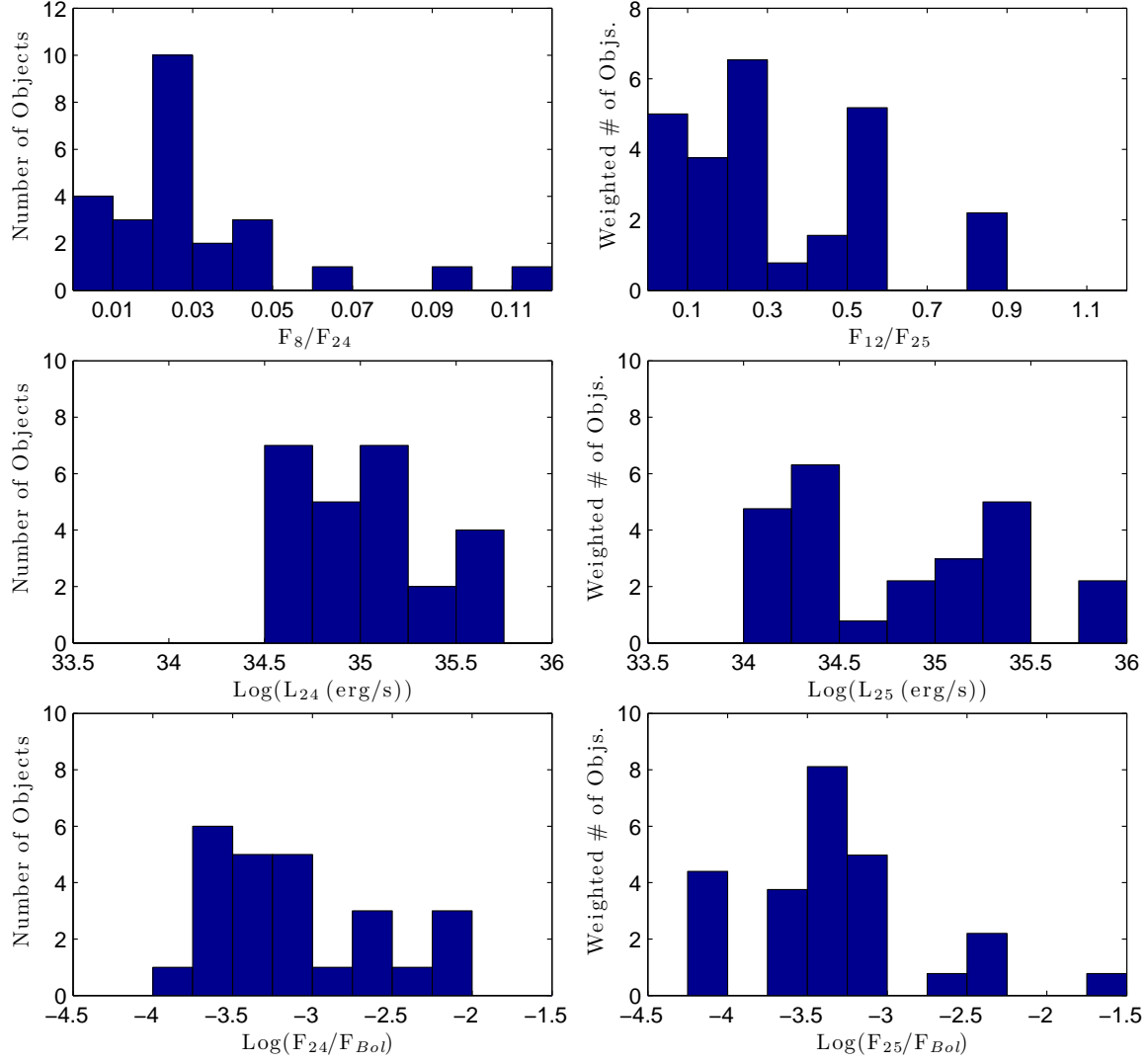


FIG. 15.— Histograms of the observable parameters displayed in Figure 17. On the left are the histograms for the SMC objects, using only those with spectral type O9–B2. On the right are the histograms for the Gaustad & van Buren (1993) sample, limited to only those objects that would have a 24 μm flux greater than $\sim 215 \mu\text{Jy}$ at the distance of the SMC. This cutoff is chosen since it is the 5- σ flux limit of the S³MC survey at 24 μm .

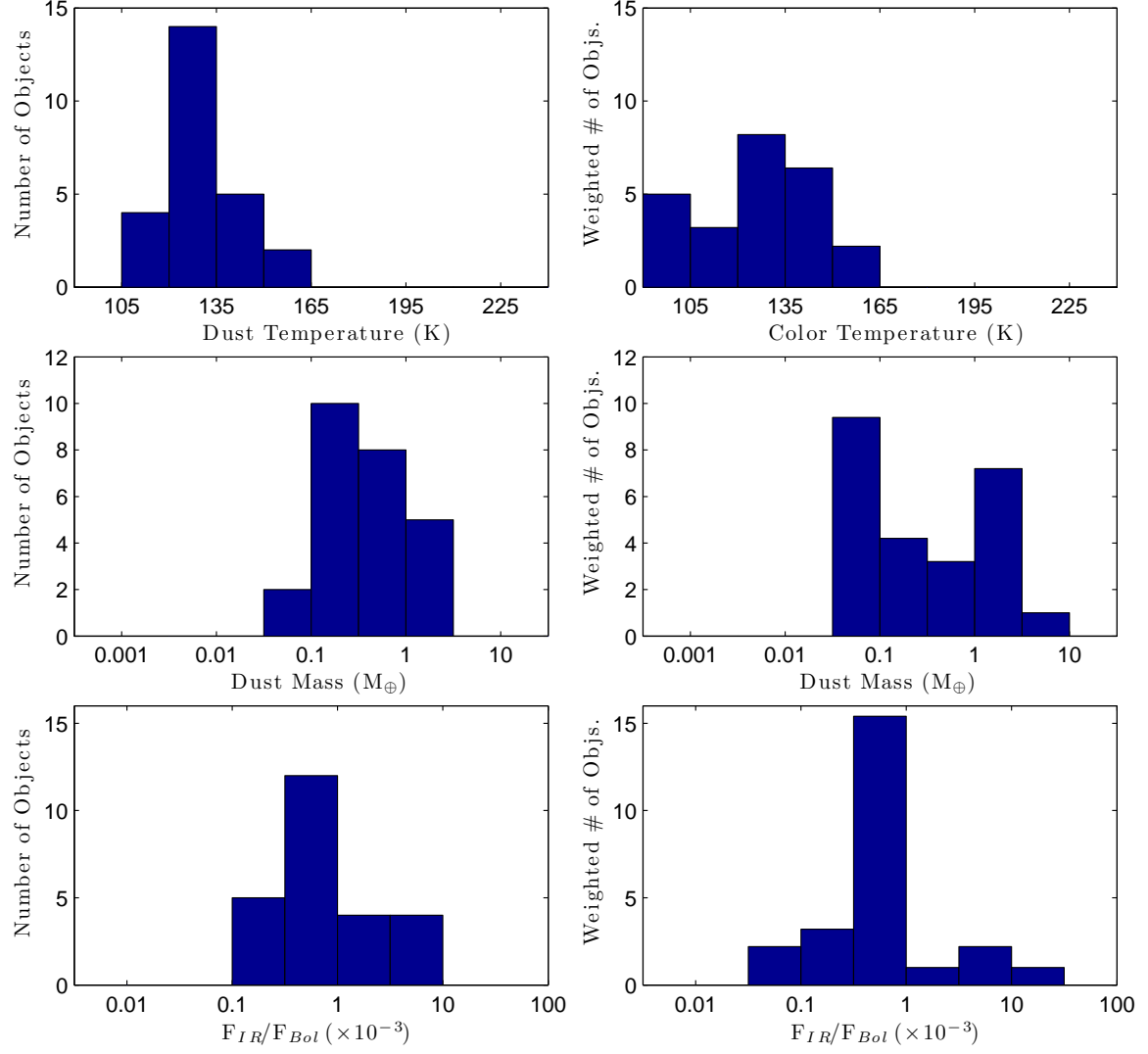


FIG. 16.— Histograms of the physical parameters in Figure 17, derived from the observable parameters in Figure 15. On the left are the histograms for the SMC objects, using only those with spectral type O9–B2. On the right are the histograms for the Gaustad & van Buren (1993) sample, limited to only those objects that would have a 24 μm flux greater than $\sim 215 \mu\text{Jy}$ at the distance of the SMC. This cutoff is chosen since it is the 5- σ flux limit of the S³MC survey at 24 μm .

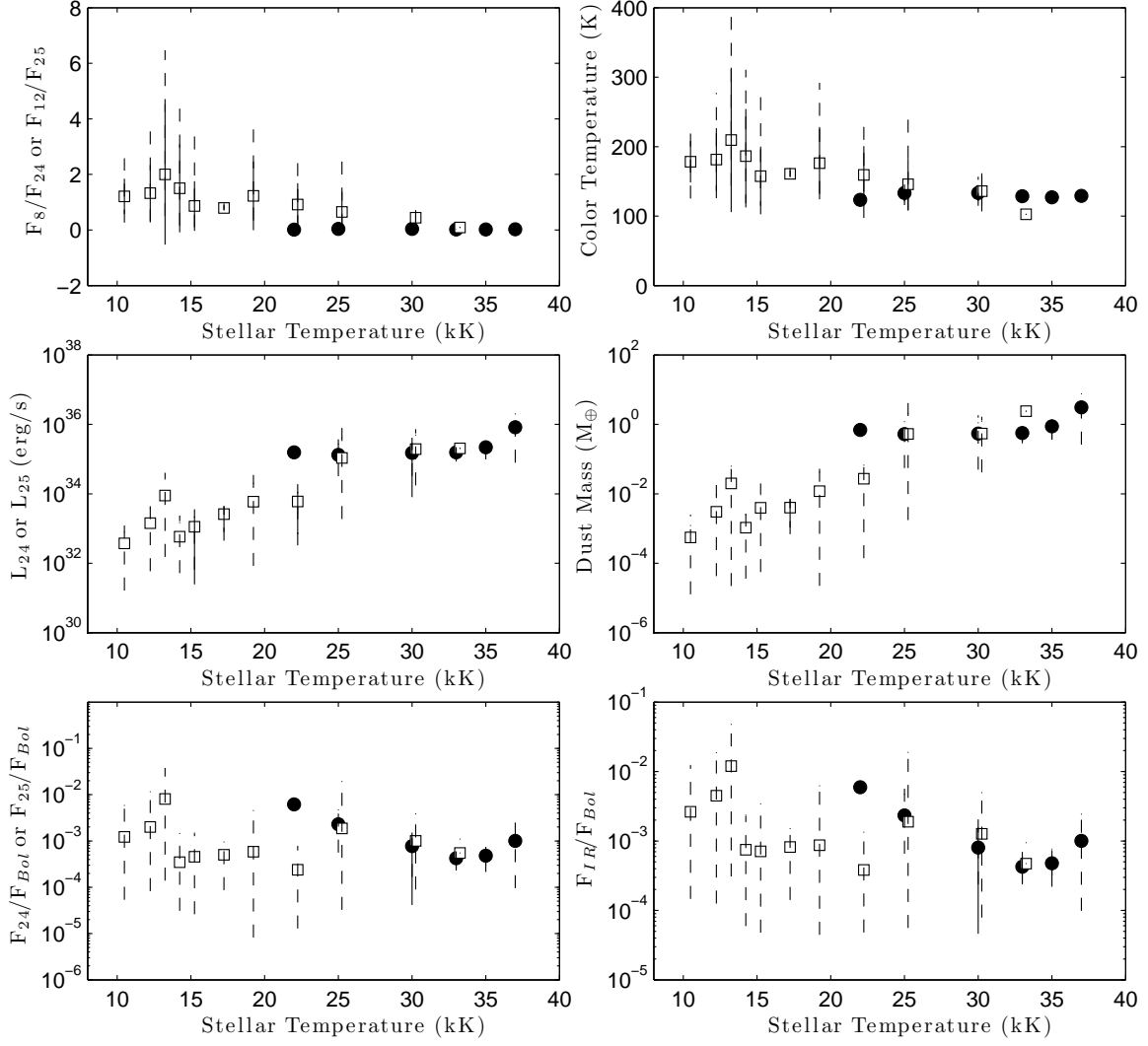


FIG. 17.— Average properties for the SMC dusty OB stars (circles) and the Gaustad & van Buren (1993) cirrus hot spots (squares) as a function of stellar temperature. On the left are the observable quantities from which the physical parameters on the right are derived. The solid bars on each point represent the standard deviation, and the dashed lines connect the maximum and minimum value for each stellar temperature. The Gaustad & van Buren (1993) points are offset in stellar temperature by +250 K for clarity. The spectral types O7–B2 correspond to stellar temperatures of 37,000 to 22,000 K. Points without bars only have one or two objects included in the average, except in the case of the F_{IR}/F_{Bol} panel. The standard deviation for this panel has a negative lower bound for all of the hot spots and for O7 (37,000 K), B0 (30,000 K), and B1 (25,000 K) in the SMC sample.

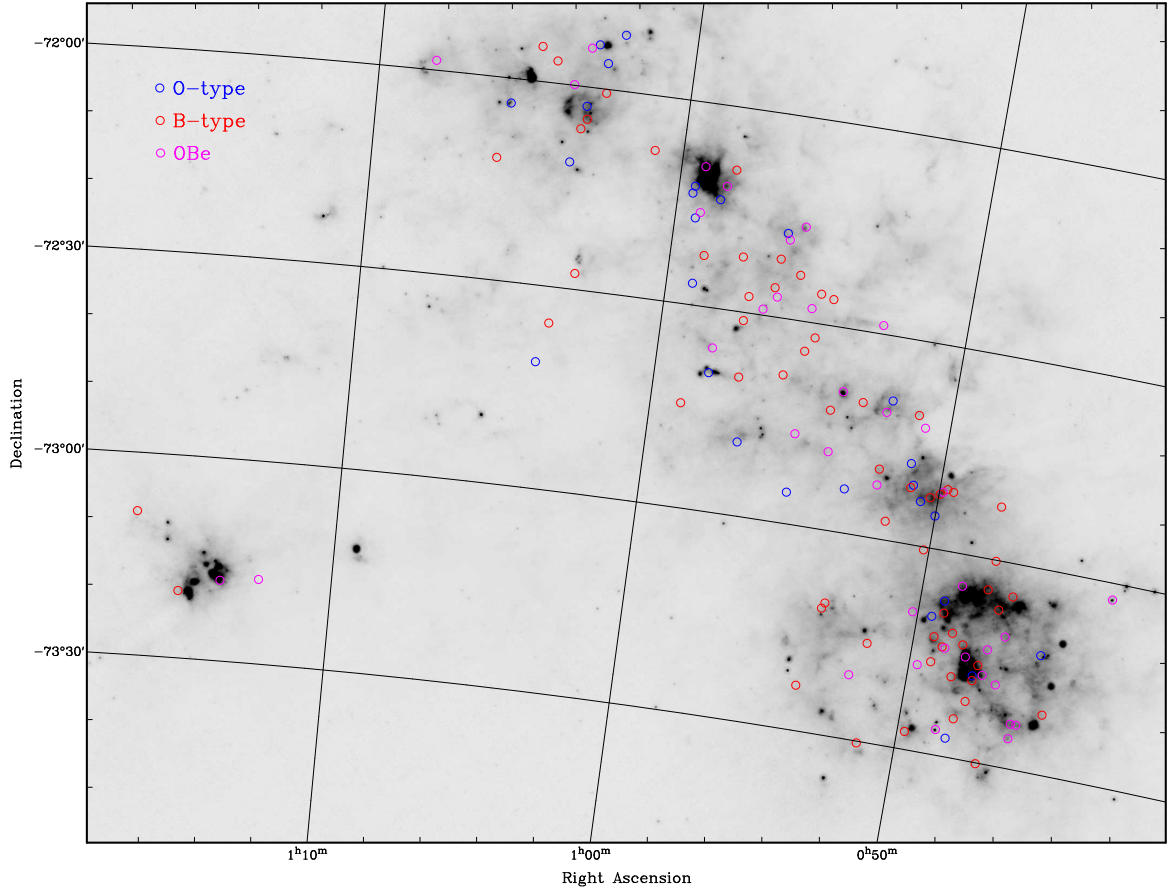


FIG. 18.— Map of the $70\text{-}\mu\text{m}$ emission (SAGE-SMC, Gordon et al. 2011) with overlain the dusty O-type stars (blue), B-type stars (red) and other, mainly OB-type emission-line stars (magenta). The latter tend towards the peak of $70\text{-}\mu\text{m}$ emission but the B-type and even O-type stars often stray away from prominent star-forming regions suggesting some may be runaways (not necessarily with a bow-shock).

TABLE 1
SMC DUSTY O AND B STARS: OPTICAL AND 2MASS DATA

ID No.	Name	RA (J2000) (deg)	Dec (J2000) (deg)	B ^a (μ Jy)	V ^a (μ Jy)	I ^a (μ Jy)	J (μ Jy)	H (μ Jy)	K (μ Jy)
B001	J004336.56–730226.80	10.90234	–73.04078	2078.39	1585.23	918.67	1088.65 ^a	564.29 ^a	827.17 ^a
B003	J004511.14–732111.95	11.29644	–73.35332	1909.53	1424.6	780.47	387.0	278.2	...
B004	J004537.37–731236.50	11.40574	–73.21014	3743.92	2976.41	1783.03	1008	573.7	391.1
B005	J004600.13–732324.54	11.50056	–73.39015	1502.89	1180.57	715.75
B006	J004610.79–732535.61	11.54496	–73.42656	2684.89	2484.81	1688.72	1339	996.1	852.6
B007	J004611.72–732325.54	11.54884	–73.39043	6530.19	5655.79	3742.47	2295.56 ^a
B009	J004655.83–730452.89	11.73266	–73.08136	3625.15	2824.18	1596.46	768.6	523.2	261.5
B010	J004656.08–731054.83	11.73367	–73.18190	8190.79	6787.24	4409.19	2667	1709	1199
B011	J004657.30–731808.71	11.73879	–73.30242	1575.16	1221.5	682.27	353.91 ^a
B013	J004707.66–733008.17	11.78192	–73.50227	5187.12	4007.68	2255.06	1099.74 ^a	749.38 ^a	...
B014	J004718.97–730711.20	11.82905	–73.11978	6590.62	5134.44	2956.37	1613	881.3	536.9
B015	J004726.74–731316.13	11.86142	–73.22115	3905.94	3351.92	1933.56	1740	1549	1125
B016	J004727.53–731705.89	11.86473	–73.28497	1945.03	1775.39	1073.39	477.85 ^a
B019	J004740.20–731548.63	11.91752	–73.26351	2780.52	2214.59	1273.97	699.7	403.9	280.5
B021	J004742.79–730009.75	11.92833	–73.00271	8800.88	7009.6	4080.92	2281	1324	849.4
B022	J004746.41–731809.93	11.94339	–73.30276	2239.37	1744.59	988.91	518.2	280.5	...
B023	J004747.53–731727.74	11.94806	–73.29104	2592.54	2333.96	1620.16	977.4	618.7	433.2
B024	J004747.93–730431.15	11.94971	–73.07532	2757.57	2144.34	1229.02	580.3	379.8	317.3
B025	J004752.03–725207.85	11.96681	–72.86885	6393.31	5755.63	3495.9	1899	1146	700.0
B026	J004752.19–732121.95	11.96750	–73.35610	3806.50	2976.41	1728.06	947.3	519.4	275.1
B028	J004808.41–731454.70	12.03507	–73.24853	2906.2	6316.74	3064.49	5376	5601	7522
B029	J004809.68–732413.06	12.04036	–73.40363	9676.67	7566.47	4141.51	2310	1308	792.0
B032	J004818.08–731312.79	12.07537	–73.22022	2196.47	1689.25	939.2	492.6	262.5	...
B033	J004818.91–732715.30	12.07881	–73.45425	6806.53	5139.17	2852.06	1425	800.0	547.9
B034	J004830.03–731809.53	12.12513	–73.30265	1872.95	1424.6	900.24	466.11 ^a	360 ^a	...
B035	J004840.43–730441.87	12.16846	–73.07830	3018.05	2662.52	1750.49	1133	687.9	434.0
B036	J004841.77–732615.25	12.17408	–73.43757	2631.03	2575.69	1516.21	1272	1047	987.9
B037	J004843.19–731147.65	12.18000	–73.19657	7239.79	5645.38	3084.31	1520	935.6	503.0
B038	J004853.00–731410.31	12.22087	–73.23620	4818.66	4011.37	2713.68	1780	1253	1029
B040	J004858.95–731403.62	12.24565	–73.23434	2295.76	2012.3	1234.69	790.1	482.5	...
B042	J004907.89–730906.30	12.28289	–73.15175	3180.72	2793.14	1618.67	988.3 ^a
B043	J004910.86–730719.66	12.29525	–73.12213	5868.49	4717.3	2555.99	1273	786.9	467.7
B044	J004916.70–731631.62	12.31962	–73.27545	5661.43	4410.55	2548.93	1344	791.9	521.8
B045	J004919.07–731247.23	12.32949	–73.21312	2638.31	2198.33	1320.56	832.7	515.6	314.4
B047	J004930.97–730952.88	12.37908	–73.16469	2255.93	1881.45	1102.45	636.9	346.0	...
B048	J004931.95–725116.88	12.38313	–72.85469	10827.45	8474.09	4906.35	2619	1574	903.5
B049	J004942.72–731718.20	12.42801	–73.28839	7470.09	6161.59	4257.54	1264.72 ^a
B051	J004944.38–725102.05	12.43493	–72.85057	1212.62	979.25	586.62
B052	J004944.32–732012.63	12.43470	–73.45601	1274.46	1115.05	733.77	437.8	263.0	...
B055	J004952.37–725131.60	12.46821	–72.85878	2336.29	1838.62	1099.41
B057	J004957.89–725154.79	12.49123	–72.86522	8752.38	5766.24	3861.52	2101	1216	735.8
B059	J005000.46–725512.36	12.50192	–72.92010	8190.79	6133.28	3670.78	2172	1295	815.82 ^a
B062	J005010.98–730943.41	12.54577	–73.16206	2399.53	1845.41	1167.24	712.0	454.1	326.2
B064	J005011.21–730026.02	12.54675	–73.00723	4259.18	3302.88	2129.9	1190	691.0	468.1
B065	J005016.35–725239.03	12.56816	–72.87751	1845.55	1444.42	875.71	477.0	306.7	255.6
B066	J005034.13–725328.17	12.64223	–72.89116	3523.11	2630.83	1473.53	681.2	413.3	262.7
B068	J005049.59–724239.96	12.70665	–72.71110	10678.89	7850.42	4454.09	2245	1317	824.0
B069	J005053.67–725116.34	12.72363	–72.85454	1759.24	1352.99	792.79	505.9	253.2	244.3
B070	J005058.13–725141.14	12.74222	–72.86143	3009.72	2194.29	1303.64	663.3	424.9	248.2
B072	J005105.15–724810.08	12.77149	–72.80280	2561.69	1925.28	1086.32	501.7	279.2	168.4
B073	J005105.83–724057.50	12.77430	–72.68264	7094.57	5177.18	2878.45	1719	933.0	632.6
B075	J005118.76–733016.19	12.82818	–73.50450	4881.19	3834.36	2106.49	1037	538.4	356.7
B076	J005131.66–731529.01	12.88192	–73.25806	2842.67	2101.32	1298.85
B077	J005137.38–725713.64	12.90577	–72.95379	8281.82	6469.83	3670.78	2010	1195	751.5
B079	J005158.09–732031.38	12.99207	–73.34205	644.65	945.57	525.72	1320	1429	2060
B080	J005202.13–723930.09	13.00888	–72.65836	6038.46	4165.75	2586.77	1339	745.3	541.4
B081	J005206.00–725209.19	13.02502	–72.86922	1918.34	1536.36	1067.48	1106	874.8	823.2
B082	J005206.44–724946.84	13.02685	–72.82968	5298.17	4204.29	2502.41	...	1153	895.2
B083	J005210.67–724119.21	13.04448	–72.68867	3497.24	2408.2	1561.56	989.2	560.7	346.4
B085	J005245.05–722844.03	13.18771	–72.47890	4366.43	4015.07	2782.01	1894	1281	855.7
B087	J005300.20–724027.84	13.25087	–72.67440	9014.18	6093.87	3518.51	1929	1137	766.9
B088	J005309.30–725331.30	13.28879	–72.89203	6812.81	4989.91	2771.78	1358	771.8	493.8
B089	J005310.59–731038.38	13.29413	–73.17733	4652.92	3699.07	2149.6	1130	615.3	413.4
B091	J005315.69–731128.17	13.31541	–73.19116	5708.55	4542.48	2656.8	1374	823.9	441.7
B092	J005342.39–732320.18	13.42664	–73.38894	2401.74	1881.45	1146.99	658.4	429.2	239.0
B093	J005342.42–723921.52	13.42678	–72.65598	2206.61	1966.5	1357.56	1379.39 ^a	920.24 ^a	654.03 ^a
B094	J005353.43–724828.58	13.47266	–72.80794	10503.31	8003.74	5128.12	3023	1773	1116
B096	J005401.98–724221.92	13.50825	–72.70609	3461.99	2533.34	1495.4	777.8	468.9	308.7
B098	J005429.76–722607.36	13.62401	–72.43538	3956.64	3296.8	2151.59	1258.02 ^a	678.42 ^a	629.79 ^a
B100	J005454.44–723209.52	13.72685	–72.53598	2283.11	1777.02	954.9	478.3	318.5	...
B101	J005455.07–722537.27	13.72946	–72.42702	6657.73	5087.37	2766.68	1446	842.4	489.7
B102	J005503.27–725521.36	13.76366	–72.92260	6145.06	4635.46	2445.45	1205.84 ^a	709.09 ^a	487.07 ^a
B103	J005504.51–724637.52	13.76883	–72.77709	9784.22	8100.15	4541.07	2484.78 ^a	1521.6 ^a	981.74 ^a
B104	J005509.36–722756.55	13.78901	–72.46571	9966.12	7996.37	4528.54	2607	1531	984.3

TABLE 1 — *Continued*

ID No.	Name	RA (J2000) (deg)	Dec (J2000) (deg)	B ^a (μ Jy)	V ^a (μ Jy)	I ^a (μ Jy)	J (μ Jy)	H (μ Jy)	K (μ Jy)
B105	J005510.66–723420.78	13.79445	–72.57244	10245.33	8528.9	5185.12	3049	1862	1130
B107	J005541.20–722320.14	13.92170	–72.38893	5645.81	4648.29	2454.47	2984.61 ^a	1963.81 ^a	1216.73 ^a
B108	J005544.60–721609.94	13.93584	–72.26943	3139.97	2316.82	1206.59	666.3	377.7	282.0
B109	J005545.75–723817.55	13.94066	–72.63821	1563.6	1189.3	653.97	422.75 ^a
B112	J005611.62–721824.26	14.04843	–72.30674	7029.53	5527.05	2878.45	1383	814.1	474.2
B115	J005617.30–721728.75	14.07210	–72.29132	3716.43	3110.95	1636.66	928.3	576.4	357.7
B116	J005620.07–722702.23	14.08366	–72.45062	2260.09	1773.75	1003.6	491.7	318.2	...
B117	J005623.53–722124.12	14.09807	–72.35670	4770.08	4402.44	2252.99	1016	580.6	353.1
B118	J005627.11–722542.88	14.11296	–72.42858	...	2638.11	1499.54	864.8	521.8	319.7
B119	J005644.27–722906.75	14.18448	–72.48521	6328.87	5557.67	3886.5	2922	2060	1465
B122	J005656.35–724906.78	14.23481	–72.81855	5486.89	4282.46	2474.9	1185	739.1	389.0
B123	J005712.13–723934.13	14.30056	–72.65976	5293.29	4239.29	2438.7	1265	711.0	426.1
B124	J005715.21–722734.30	14.31341	–72.45953	4423.09	3348.83	1879.14	992.9	575.3	363.7
B125	J005719.21–723112.90	14.33005	–72.52025	3641.88	2938.28	1626.14	949.9	501.5	298.1
B126	J005737.27–722154.32	14.40530	–72.36509	8849.65	6843.73	3763.21	1959	1171	639.6
B127	J005811.84–723552.65	14.54937	–72.59796	7779.04	6457.93	3704.75	1941	1147	697.5
B128	J005812.38–723934.81	14.55161	–72.65967	6242.03	4840.53	2733.75	1421	817.9	525.7
B129	J005813.89–720919.51	14.55790	–72.15542	3631.83	2911.34	1606.79	790.1	470.7	340.4
B132	J005827.49–721153.91	14.61457	–72.19831	2827	2306.18	1413.7	795.2	492.8	297.8
B135	J005837.02–721359.91	14.65429	–72.23331	4173.75	3312.02	1967.7	1130	733.0	410.7
B136	J005853.66–722230.75	14.72359	–72.37521	1838.76	1508.32	904.4	527.8	411.1	405.8
B137	J005859.13–724434.11	14.74641	–72.74281	9224.14	7239.24	4114.89	2061	1244	807.5
B139	J005908.61–722648.58	14.78591	–72.44683	2239.37	1703.31	942.67	501.7	308.4	...
B140	J005912.41–721617.86	14.80172	–72.27163	1508.43	1215.89	713.11	679.3	461.2	379.8
B141	J005913.87–720927.32	14.80780	–72.15759	1675.43	1560.61	851.84	1060.93 ^a	875.59 ^a	530.63 ^a
B142	J005920.70–721710.89	14.83629	–72.28636	9014.18	7003.14	3940.57	1990	1264	794.9
B144	J005928.82–721231.57	14.87009	–72.20877	4480.5	3395.42	1873.95	877.6	577.4	280.8
B145	J005931.78–721334.96	14.88242	–72.22638	3433.41	2580.44	1400.74	708.7	487.4	353.8
B148	J010055.17–720804.66	15.22989	–72.13463	6825.37	5082.68	2784.57	1474	823.9	537.9
B152	J010217.77–715143.09	15.57407	–71.86197	5027.2	4048.49	2189.57	1214	705.8	405.1
B154	J010241.58–720036.14	15.67326	–72.01004	2115.08	1686.14	910.25	458.87 ^a
B156	J010245.09–715612.26	15.68790	–71.93674	6670	5603.93	3400.62	1981	1281	806.0
B159	J010300.05–722738.19	15.75023	–72.46061	5172.8	3816.74	2068.04	1060	519.9	373.2
B160	J010304.84–715335.77	15.77017	–71.89327	1500.12	1461.82	830.92	534.2	294.0	392.64 ^a
B161	J010312.30–720445.66	15.80126	–72.07935	...	2241.26	1222.25	620.1	391.8	...
B163	J010315.76–720251.61	15.81567	–72.04767	5101.83	3695.67	1884.34	960.5	563.8	335.1
B165	J010318.91–715413.35	15.82883	–71.90371	5879.31	5096.75	3036.4	1845	1167	790.6
B167	J010322.54–720616.59	15.84393	–72.10461	1219.34	1441.76	876.51	899.7	632.6	354.8
B169	J010336.20–721120.32	15.90086	–72.18898	3938.46	2938.28	1594.99	775.7	440.9	260.1
B172	J010339.23–723523.13	15.91347	–72.58976	1749.55	1385.78	812.75	471.3	375.9	...
B175	J010344.37–715953.37	15.93491	–71.99816	1311.37	1123.29	713.77	452.6	308.4	...
B177	J010356.40–724117.95	15.98504	–72.68832	2790.78	2029.05	1045.1	436.6	274.1	...
B179	J010421.39–715642.39	16.08913	–71.94511	...	5851.85	3271.59	1694	952.1	631.4
B182	J010452.94–715449.28	16.22062	–71.91369	12397.27	8357.82	5118.69	2564	1540	973.5
B183	J010541.21–720340.39	16.42175	–72.06122	5031.83	3675.3	2217.98	1499	886.1	634.9
B184	J010557.47–721154.24	16.48946	–72.19840	5050.4	3624.88	1955.05	969.37 ^a	564.81 ^a	418.02 ^a
B188	J010812.07–715833.34	17.05033	–71.97593	4468.13	3278.63	1694.96	885.7	583.3	292.6
B190	J011229.71–731729.83	18.12382	–73.29162	8632.29	4492.55	2794.85	4542	3332	2509
B191	J011348.83–731805.04	18.45350	–73.30140	7916.37	6651.09	4245.79	1835.22 ^a	1034.43 ^a	917.9 ^a
B192	J011513.70–732003.29	18.80712	–73.33425	8537.41	6369.32	3413.17	1636	997.9	585.5
B193	J011647.69–730839.62	19.19872	–73.14434	5230.29	4262.78	2337.54	1228	757.0	462.5

^a Original S³MC data point.

TABLE 2
SMC DUSTY O AND B STARS: SPITZER DATA

ID No.	3.6 μm (μJy)	$\sigma_{3.6\mu\text{m}}$ (μJy)	4.5 μm (μJy)	$\sigma_{4.5\mu\text{m}}$ (μJy)	5.8 μm (μJy)	$\sigma_{5.8\mu\text{m}}$ (μJy)	8.0 μm (μJy)	$\sigma_{8.0\mu\text{m}}$ (μJy)	24 μm^{a} (μJy)	$\sigma_{24\mu\text{m}^{\text{a}}}$ (μJy)	70 μm^{a} (μJy)	$\sigma_{70\mu\text{m}^{\text{a}}}$ (μJy)
B001	444.40 ^b	2.93	198102.30	624.29
B003	58.53	2.28	44.12	2.51	930.76	26.62
B004	159.10	4.02	99.99	3.94	98.28 ^b	8.64	1684.34	26.40
B005	189.40	7.51	168.70	6.12	382.80	23.00	666.20	33.63	4215.01	42.52
B006	263.10	14.05	238.36 ^b	1.74	287.10	17.45	659.70	40.85	22090.02	111.60
B007	575.10	9.76	412.60	9.30	323.90	14.23	198.40	12.74	1647.90	29.82
B009	142.30	6.08	96.72	4.76	92.00 ^b	9.48	2500.48	31.08
B010	661.70	14.72	500.50	11.84	478.50	18.28	584.80	31.21	7382.77	55.72
B011	51.80	1.96	39.78	2.78	2087.20	28.72
B013	167.60	3.61	110.60	3.62	1149.26	28.52
B014	225.30	4.66	142.00	4.02	123.76 ^b	9.19	87.58 ^b	11.13	1948.75	28.46
B015	485.20	14.90	319.70	12.28	238.50	15.34	158.24 ^b	14.35	4843.77	46.41
B016	114.80	4.17	83.30	4.40	211.60 ^b	14.35	7047.57	52.57
B019	118.30	3.81	92.86	3.76	2534.84	54.48
B021	331.90	6.01	214.00	4.20	155.40	12.08	104.88 ^b	8.54	1093.05	27.72
B022	79.59	2.59	67.77	2.90	93.73 ^b	9.06	186.10	11.38	6160.64	58.06
B023	178.60	3.62	162.40	5.56	229.90	13.47	790.30	27.31	39214.47	204.24
B024	88.11	2.55	58.20	1.84	55.02 ^b	9.16	1093.05	29.29
B025	282.60	6.98	180.80	3.83	138.32 ^b	8.68	80.96 ^b	10.03	835.30	28.19
B026	140.80	3.77	90.96	3.72	1002.48	27.70
B028	9138.00	466.30	14030.00	513.70	37120.00	1022.00	100300.00	8321.00	1632288.00 ^b	1264.81	11107800.00 ^b	36590.40
B029	319.80	8.72	186.60	5.31	178.20	13.72	125.12 ^b	13.98	5955.56	46.19
B032	76.24	2.36	48.01	2.97	3525.87	91.61
B033	208.50	4.38	133.10	3.82	119.21 ^b	9.19	1591.69	25.90
B034	86.66	2.59	62.21	2.99	1414.72	31.51
B035	204.30	4.58	128.90	3.61	75.53 ^b	8.78	721.31 ^b	60.49
B036	1836.80 ^b	27.55	983.10	39.52	3013.00	104.30	7000.00	432.70	256606.50	591.81	1687950.00 ^b	8396.19
B037	231.70	4.55	147.90	4.19	141.96 ^b	8.34	1380.37	28.68
B038	619.30	10.64	498.10	13.19	402.40	12.17	274.60	11.75	726.10	28.66
B040	133.80	3.67	84.04	4.17	729.74	55.17
B042	161.60	4.59	115.30	4.05	152.88 ^b	8.34	298.70	17.57	7348.42	47.92
B043	188.00	3.99	116.30	3.88	106.47 ^b	8.22	90.80 ^b	12.88	3146.94	32.16
B044	208.90	4.30	134.20	3.80	102.83 ^b	6.18	751.91 ^b	64.57
B045	135.70	2.91	87.31	3.59	1661.44	30.26
B047	118.70	3.30	103.50	4.81	114.66 ^b	6.97	99.36 ^b	12.24	3603.94	37.27
B048	391.10	6.55	251.50	5.06	173.60	17.48	157.00	11.22	2900.23	35.98
B049	1217.00	25.07	922.20	19.78	664.50	17.57	478.80	14.78	3100.10	43.77
B051	47.97	1.97	34.55	2.44	563.18	41.64
B052	69.03	3.48	52.24	2.32	1175.29	24.27
B055	90.66	2.93	68.99	2.85	180.80	15.15	12804.30	117.53
B057	311.40	6.36	206.00	5.53	174.72 ^b	9.92	192.20	12.72	7842.89	75.97
B059	339.20	9.42	215.70	4.84	197.10	18.82	105.80 ^b	12.33	2094.49	29.79
B062	150.40	3.46	112.10	4.10	88.82 ^b	6.36	139.84 ^b	12.33	2556.70	32.02
B064	203.10	4.37	127.60	3.50	111.93 ^b	8.63	45.17 ^b	11.22	1308.54	26.49
B065	74.88	2.12	53.21	3.18	603.16	34.53
B066	108.70	3.69	65.00	2.60	90.73 ^b	8.52	122.36 ^b	12.24	4538.76	46.96
B068	428.00	7.25	321.90	8.50	262.60	11.26	202.10	11.29	1424.09	25.89
B069	70.29	2.74	56.89	2.86	802.61	58.30
B070	102.00	3.16	73.00	3.23	71.12 ^b	12.24	1229.42	29.92
B072	77.25	2.10	55.66	2.23	101.20 ^b	12.24	2370.36	29.36
B073	218.70	5.25	133.20	4.86	114.66 ^b	6.50	97.52 ^b	11.59	5202.92	33.44
B075	168.20	5.22	108.40	4.76	10368.36	56.60
B076	96.57	3.35	66.32	2.62	593.37	33.31
B077	287.90	8.23	180.10	4.98	1106.58	24.86
B079	3343.00	83.64	4702.00	69.86	8568.00	107.40	23370.00	213.00	123670.80	436.18
B080	199.70	3.73	129.90	4.72	109.20 ^b	5.93	156.80	16.59	6383.41	35.59
B081	445.60	8.69	373.80	7.63	302.10	11.44	236.90	9.44	870.07	28.67
B082	173.70	3.95	119.20	4.18	98.28 ^b	8.72	197.60	21.12	6613.47	69.29
B083	135.20	3.08	96.48	4.87	107.38 ^b	5.76	854.04	34.96
B085	469.30	8.46	337.70	13.86	230.20	11.22	169.70	28.80	693.51	27.76
B087	308.50	5.90	199.00	5.07	160.16 ^b	7.50	120.52 ^b	9.20	3015.78	30.47
B088	204.30	4.36	124.70	3.38	91.00 ^b	9.28	74.52 ^b	11.22	1408.47	27.68
B089	179.50	4.20	115.00	2.91	84.45 ^b	8.91	50.97 ^b	9.08	768.26	32.27
B091	214.90	5.42	136.60	3.53	118.30 ^b	9.28	67.90 ^b	10.58	430.97	33.31
B092	115.40	3.08	72.07	3.09	79.81 ^b	8.00	687.06	49.97
B093	417.76 ^b	3.89	281.79 ^b	1.27	535.99 ^b	10.56	51925.08	181.97
B094	493.80	8.59	363.70	7.00	273.30	11.54	263.20	9.89	4334.72	46.56
B096	116.10	2.82	76.57	2.27	68.43 ^b	6.29	58.60 ^b	8.72	796.16	25.82

TABLE 2 — *Continued*

ID No.	3.6 μm (μJy)	$\sigma_{3.6\mu\text{m}}$ (μJy)	4.5 μm (μJy)	$\sigma_{4.5\mu\text{m}}$ (μJy)	5.8 μm (μJy)	$\sigma_{5.8\mu\text{m}}$ (μJy)	8.0 μm (μJy)	$\sigma_{8.0\mu\text{m}}$ (μJy)	24 μm^{a} (μJy)	$\sigma_{24\mu\text{m}^{\text{a}}}$ (μJy)	70 μm^{a} (μJy)	$\sigma_{70\mu\text{m}^{\text{a}}}$ (μJy)
B098	227.20	5.41	152.40	4.26	94.76 ^b	13.34	582.02	22.55
B100	70.68	2.20	47.07	2.25	1319.99	26.75
B101	210.60	4.30	133.70	4.17	115.57 ^b	9.10	727.35	26.19
B102	194.80	8.24	117.40	4.12	1660.39	25.78
B103	486.08 ^b	4.87	284.82 ^b	1.16	264.81 ^b	9.74	159.16 ^b	9.38	870.28	32.01
B104	427.40	8.06	280.60	6.77	209.60	11.90	168.90	11.31	655.83	32.27
B105	482.60	8.98	345.80	7.71	211.60	12.35	136.60	13.50	2679.53	29.50	72527.40 ^b	10291.05
B107	240.70	4.89	183.90	4.96	188.37 ^b	8.09	225.10	14.99	1967.49	29.69	48787.20 ^b	2308.68
B108	99.76	3.96	65.54	9.10	7553.50	53.29
B109	52.32	1.93	32.05	2.12	1467.81	24.17
B112	202.80	3.69	124.30	5.38	99.19 ^b	7.28	101.20 ^b	16.28	1660.39	28.11
B115	176.80	5.20	117.90	5.42	106.47 ^b	6.99	94.76 ^b	19.14	4382.61	36.25
B116	86.94	2.53	56.00	2.42	638.55	34.38
B117	146.20	2.59	86.68	2.69	66.52 ^b	6.03	501.76	34.35
B118	148.90	3.87	101.70	4.08	91.91 ^b	8.64	1270.02	25.91
B119	600.70	13.71	435.50	8.94	352.80	17.41	245.40	11.80	901.51	30.18
B122	207.50	4.53	131.20	4.25	136.50 ^b	8.47	1361.63	23.57
B123	195.60	4.59	132.60	5.01	127.40 ^b	8.65	766.28	24.85
B124	135.60	3.29	87.41	3.56	74.44 ^b	8.04	624.60	34.35
B125	143.80	3.85	98.06	5.69	1465.73	29.20
B126	297.10	5.27	192.60	4.27	140.14 ^b	6.91	81.70 ^b	10.76	661.03	31.23
B127	628.00	10.72	447.10	8.66	360.40	14.61	263.40	9.61	1441.78	27.39
B128	206.20	5.18	135.30	4.07	144.69 ^b	9.83	107.64 ^b	12.97	2709.72	33.50
B129	123.20	3.59	83.92	2.78	99.19 ^b	9.83	132.10	15.81	2466.13	28.99
B132	135.20	5.09	96.28	4.71	104.65 ^b	9.83	190.60	20.00	12814.71	87.02
B135	189.30	4.48	118.40	3.75	131.04 ^b	9.37	88.96 ^b	12.33	2993.92	34.81
B136	228.80	10.10	164.80	7.40	143.78 ^b	7.60	81.42 ^b	11.13	579.84	31.23
B137	319.90	8.71	206.80	5.76	158.10	15.93	87.40 ^b	12.33	754.93	25.00
B139	65.09	2.06	50.48	2.37	58.24 ^b	6.93	52.26 ^b	9.57	1522.98	26.40
B140	211.40	5.08	161.50	4.86	137.41 ^b	9.83	86.02 ^b	12.70	675.40 ^b	62.44
B141	730.23 ^b	1.52	9752.00 ^b	49.40	136371.00	514.46
B142	304.40	6.22	193.40	5.10	132.30	13.08	86.11 ^b	12.70	2992.88	31.77
B144	145.80	3.42	87.71	3.58	82.90 ^b	8.60	102.12 ^b	15.18	2608.75	35.49
B145	103.20	2.75	71.58	3.16	100.10 ^b	8.22	189.20	11.01	3907.91	49.22
B148	212.30	3.71	139.20	3.62	126.49 ^b	9.46	85.38 ^b	14.08	927.84	27.39
B152	174.90	3.71	110.30	4.02	68.80 ^b	8.79	2816.95	29.05
B154	101.60	2.56	81.33	3.06	73.35 ^b	6.89	1415.76	29.00
B156	342.40	8.35	210.70	5.29	182.00 ^b	11.38	124.80	17.24	2463.01	32.10
B159	147.20	3.55	96.16	2.31	104.65 ^b	9.19	55.02 ^b	8.81	1303.33	27.99
B160	87.84	2.79	67.16	2.60	240.90	12.10	9942.59	61.82
B161	87.86	1.97	56.74	2.17	64.97 ^b	6.17	2092.41	35.31
B163	139.50	2.98	94.13	2.71	118.30 ^b	7.46	159.70	10.80	5640.14	45.03
B165	310.70	5.42	203.70	4.86	173.81 ^b	8.41	104.88 ^b	12.24	1355.38	27.62
B167	183.40	4.12	118.60	3.13	1087.85	55.17
B169	118.40	4.67	79.94	2.77	1088.89	26.06
B172	98.63	4.45	81.56	4.29	537.16	33.31
B175	88.11	2.95	65.13	3.51	1009.46	26.55	75141.00 ^b	3016.53
B177	66.51	2.35	49.52	2.59	1630.21	40.73
B179	257.40	4.99	154.90	4.56	148.33 ^b	8.78	2327.68	29.01	41055.30 ^b	2123.55
B182	378.10	7.24	246.80	5.58	173.30	12.55	125.12 ^b	13.06	1099.30	23.78
B183	239.40	5.89	167.00	6.22	181.09 ^b	10.83	280.40	13.41	12679.38	168.64
B184	141.30	6.19	93.57	4.53	711.11	36.93
B188	131.60	5.57	80.09	3.15	3050.13	29.75
B190	868.70	15.06	714.40	11.39	591.50	17.26	451.40	12.28	617.21	26.92
B191	872.64 ^b	2.21	5805.20 ^b	38.00	135121.80	689.04
B192	251.90	5.55	160.90	4.36	142.87 ^b	12.19	960.74	25.23
B193	183.90	4.07	122.80	3.47	1018.72	26.20

^a Includes correction factor from MIPS to IRAC scale.^b Original S³MC data point.

TABLE 3
MAIN SEQUENCE STELLAR PROPERTIES AND SPECTRAL CLASSIFICATION
SCHEME

SpT	T _{eff} (10 ³ K)	Radius (R _☉)	Mass (M _☉)	L _{bol} (10 ³ L _☉)	Slope	BC	Criteria
O6	39	12.2	30.5	309.0	−2.91	−3.72	He II 4686, 4541 Å, He I+He II 4026 ∼ He II 4200 Å
O7	37	11.3	27.3	213.3	−2.91	−3.54	He II 4686, 4200 Å, He II 4541 Å ∼ He I 4471 Å
O8.5	34	9.9	22.8	118.4	−2.91	−3.27	He II 4686, 4200 Å, He II 4541 Å ∼ He I 4387 Å
O9	33	9.5	21.5	96.3	−2.91	−3.18	He II 4686, He II 4200 Å ∼ He I 4143 Å
B0	30	8.3	17.8	50.3	−2.89	−2.98	He II 4686, 4541 Å, weak He II 4200 Å
B0.5	27	7.2	14.5	24.8	−2.86	−2.60	Weak He II 4686 Å, no He II 4200, 4541 Å
B1/1.5	25	6.5	12.5	15.0	−2.84	−2.41	Si IV 4088, 4116 Å
B2/B3	22	5.6	10.0	6.6	−2.79	−2.11	Si III 4553 Å
B5/B8	15	3.8	5.4	0.6	−2.67	−1.24	Si II 4128/4132 Å, no Si III 4553 Å
B9	10	2.8	3.2	0.1	−2.52	−0.30	Si II 4128/4132 Å, Mg II 4481 Å > He I 4471 Å

TABLE 4
SMC DUSTY O AND B STARS: SPECTRAL TYPE, RADIAL VELOCITY AND
IDENTIFICATION

This Work No.	SpT ^a	Literature		source ^b	v_{rad} H I (km s ⁻¹)	Identification
		SpT	v_{rad} (km s ⁻¹)			
B001	Em					Planetary Nebula
B003	B0–B2					
B004	O9					
B005	...					Eclipsing binary
B006	...					
B007	OBe					
B009	B0–B2					
B010	OBe					Emission-line star
B011	...					
B013	B0					
B014	B0–B2					
B015	OBe?					
B016	OBe					
B019	B0–B2					
B021	B0	B1–2 II	150 ± 6	EH08	136	
B022	B0					
B023	O7					
B024	B0–B2					Eclipsing binary
B025	B0–B2					
B026	B0–B2					
B028	Em					Compact H II region
B029	B0					
B032	B1					
B033	O7–O9					
B034	B0					
B035	OBe?					O6 Iaf (see section 3)
B036	Em	B0 V?		S		Young stellar object
B037	B1					
B038	OBe					
B040	B0–B2					
B042	B0					
B043	O9					
B044	B0					
B045	B1					
B047	O7					
B048	B2	B0.5 IV	103 ± 9	EH08	119, 141	
B049	OBe					
B051	B0					
B052	B0					
B055	OBe					Emission-line star
B057	B0–B2	B2		S		
B059	O9	B3		S		
B062	OBe?					
B064	B0	B1–3 III–V(e)		C11		X-ray binary
B065	B1					
B066	O9					
B068	OBe	B2?		S		Emission-line star
B069	O7–O9					
B070	B0–B2					
B072	O8.5					
B073	B1					Eclipsing binary
B075	B0–B2					Eclipsing binary
B076	B1					
B077	B0–B2					
B079	Em					Planetary Nebula
B080	O8.5					Emission-line star
B081	OBe					Emission-line star
B082	B1					Emission-line star
B083	OBe?	B1–5 III	165 ± 6	EH08	125, 159	
B085	OBe	O9–B0e		A09		X-ray binary
B087	B0					
B088	O7					
B089	B1					
B091	B0–B2					
B092	B0					Eclipsing binary
B093	...					Eclipsing binary
B094	Em	B2?		S		Emission-line star
B096	B0					Eclipsing binary
B098	B1					
B100	B1	B0.5 V	124	H08, E06	129, 160–180	
B101	B5	B1–5 II	168 ± 17	EH08	134, 167	

TABLE 4 — *Continued*

This Work No.	SpT ^a	Literature		source ^b	v_{rad} H I (km s ⁻¹)	Identification
		SpT	v_{rad} (km s ⁻¹)			
B102	O9					
B103	OBe	B1 II		S		
B104	OBe	B1–3 II	165 ± 10	EH08	128, 163	
B105	B2	B3?		S		
B107	B1					Emission-line star
B108	...	B2 IV	137 ± 10	M07	137, 165	
B109	B0–B2					Eclipsing binary
B112	...					
B115	O7–O9	O9 V	134 ± 10	M07	136, 164	
B116	OBe	B2 III(IVe?)	151	H08, S, E06	130, 170	
B117	B0–B2	B0.5 V		E06		Spectroscopic binary
B118	B0	B2 II	130	H08, E06	130, 166	
B119	OBe	B0 III	148 ± 10, 159	M07, E06	129, 167	
B122	O7–O9					Eclipsing binary?
B123	B0–B2					
B124	B0	B1 V, B1–2 III	143 ± 3	H08, EH08	131, 168	
B125	B1					
B126	B1	B0 IV, B0.5 IV	176 ± 10, 182 ± 15	M07, EH08	131, 160–180	
B127	OBe					
B128	O9					
B129	B0–B2	B0 V	172	H08, E06	166	
B132	OBe?	B0.5 V	176	H08, E06	180	Emission-line star
B135	O7–O9					
B136	B0					
B137	B1	B1–3 II	142 ± 10	EH08	130, 146, 177	Eclipsing binary
B139	O9					
B140	OBe					
B141	Em	B0 V		H08		Emission-line star
B142	O8.5	O7 IIIIn((f))	208	H08, E06	131, 173	
B144	O7–O9					X-ray source within 5''
B145	O7–O9	O7 Vn	250	H08, E06	130, 175	
B148	B0					
B152	O7–O9					
B154	B1					
B156	O7–O9	B1		S		
B159	B0					
B160	O7–O9					Emission object within 5''
B161	B0					
B163	O7–O9					
B165	OBe?					
B167	A0					
B169	O7–O9					
B172	B0–B2					
B175	...					
B177	O7–O9	O9 V	123 ± 8	EH08	131, 185	
B179	B0					
B182	B0					
B183	O7–O9					Emission object at 3''
B184	B0–B2	B0.5 V	139 ± 14	EH08	144, 187	Eclipsing binary
B188	OBe?					
B190	OBe					Emission-line star at 2''
B191	...	Be?		S		
B192	B0–B2	B1–3 II	196 ± 14	EH08	144, 179	
B193	B0					

^a "Em" denotes objects with forbidden emission lines. "OBe" denotes Be stars. "OBe?" denotes stars with unusually weak H α absorption. No spectral type information indicates that the spectra were difficult to extract.

^b A09 = Antoniou et al. (2009); C11 = Coe et al. (2011); E06 = Evans et al. (2006); EH08 = Evans & Howarth (2008); H08 = Hunter et al. (2008); M07 = Martayan et al. (2007); S = Simbad.

TABLE 5
SMC DUSTY O AND B STARS: 4.5, 8, AND 24 μm EXCESSES

No.	4.5 μm		8.0 μm		24 μm		K-[24]
	Excess (μJy)	Ratio ^a	Excess (μJy)	Ratio ^a	Excess (μJy)	Ratio ^a	
B001	340 \pm 13	3.27 \pm 0.53	198098 \pm 624	41436 \pm 5181	10.86
B003	7 \pm 5	0.19 \pm 0.15	929 \pm 27	547 \pm 64	...
B004	12 \pm 5	0.14 \pm 0.06	1681 \pm 26	467 \pm 19	6.49
B005	137 \pm 7	4.40 \pm 0.61	655 \pm 34	60.5 \pm 7.3	4214 \pm 43	2935 \pm 318	...
B006	110 \pm 13	0.86 \pm 0.19	615 \pm 41	13.9 \pm 1.8	22084 \pm 112	3756 \pm 387	8.44
B007	193 \pm 26	0.88 \pm 0.21	122 \pm 15	1.6 \pm 0.3	1638 \pm 30	162 \pm 18	...
B009	23 \pm 9	0.32 \pm 0.16	67 \pm 10	2.6 \pm 0.5	2497 \pm 31	740 \pm 80	7.36
B010	246 \pm 29	0.96 \pm 0.21	496 \pm 33	5.6 \pm 0.8	7371 \pm 56	629 \pm 65	6.88
B011	6 \pm 6	0.18 \pm 0.22	2086 \pm 29	1342 \pm 231	...
B013	12 \pm 12	0.12 \pm 0.14	1145 \pm 29	275 \pm 33	...
B014	-12 \pm 16	-0.08 \pm 0.10	34 \pm 12	0.6 \pm 0.3	1942 \pm 28	274 \pm 28	6.31
B015	153 \pm 21	0.92 \pm 0.21	101 \pm 16	1.7 \pm 0.4	4836 \pm 46	633 \pm 66	6.49
B016	38 \pm 8	0.82 \pm 0.28	196 \pm 15	12.4 \pm 2.1	7045 \pm 53	3357 \pm 488	...
B019	26 \pm 8	0.39 \pm 0.16	2532 \pm 54	824 \pm 90	7.30
B021	10 \pm 21	0.05 \pm 0.11	36 \pm 11	0.5 \pm 0.2	1084 \pm 28	126 \pm 13	5.18
B022	21 \pm 6	0.46 \pm 0.17	170 \pm 12	10.9 \pm 1.5	6159 \pm 58	3139 \pm 349	...
B023	77 \pm 7	0.90 \pm 0.10	762 \pm 27	26.8 \pm 1.5	39211 \pm 204	11244 \pm 481	9.80
B024	3 \pm 6	0.05 \pm 0.11	36 \pm 9	1.9 \pm 0.6	1091 \pm 29	428 \pm 44	6.25
B025	-1 \pm 19	-0.00 \pm 0.10	18 \pm 12	0.3 \pm 0.2	827 \pm 28	99 \pm 11	5.10
B026	0 \pm 10	0.00 \pm 0.11	998 \pm 28	240 \pm 25	6.31
B028 ^b	13516 \pm 517	26.31 \pm 3.17	100122 \pm 8321	561.8 \pm 77.6	1632264 \pm 1265	69138 \pm 7623	10.75
B029	-20 \pm 22	-0.10 \pm 0.10	55 \pm 16	0.8 \pm 0.3	5947 \pm 46	680 \pm 71	7.10
B032	1 \pm 6	0.02 \pm 0.13	3524 \pm 92	1629 \pm 184	...
B033	9 \pm 6	0.07 \pm 0.05	1587 \pm 26	312 \pm 11	6.07
B034	20 \pm 7	0.49 \pm 0.24	1413 \pm 32	801 \pm 123	...
B035	21 \pm 13	0.19 \pm 0.15	716 \pm 60	144 \pm 21	5.46
B036 ^b	862 \pm 42	7.09 \pm 0.91	6958 \pm 433	165.0 \pm 20.3	256601 \pm 592	45936 \pm 4839	10.95
B037	3 \pm 16	0.02 \pm 0.11	1374 \pm 29	206 \pm 22	6.00
B038	328 \pm 22	1.93 \pm 0.31	216 \pm 13	3.7 \pm 0.5	718 \pm 29	92 \pm 10	4.53
B040	9 \pm 9	0.11 \pm 0.14	726 \pm 55	209 \pm 28	...
B042	27 \pm 11	0.30 \pm 0.16	269 \pm 18	9.0 \pm 1.3	7345 \pm 48	1963 \pm 236	...
B043	5 \pm 5	0.05 \pm 0.05	54 \pm 13	1.5 \pm 0.4	3142 \pm 32	692 \pm 25	6.98
B044	14 \pm 13	0.11 \pm 0.12	747 \pm 65	147 \pm 20	5.31
B045	8 \pm 9	0.10 \pm 0.13	1658 \pm 30	453 \pm 51	6.72
B047	48 \pm 6	0.86 \pm 0.13	81 \pm 12	4.4 \pm 0.7	3602 \pm 37	1585 \pm 90	...
B048	-15 \pm 28	-0.06 \pm 0.10	62 \pm 15	0.6 \pm 0.2	2887 \pm 36	216 \pm 22	6.17
B049	736 \pm 28	3.96 \pm 0.55	414 \pm 16	6.4 \pm 0.8	3092 \pm 44	362 \pm 40	5.88
B051	11 \pm 3	0.47 \pm 0.18	562 \pm 42	567 \pm 71	...
B052	13 \pm 5	0.33 \pm 0.16	1174 \pm 24	708 \pm 80	...
B055	21 \pm 6	0.44 \pm 0.16	164 \pm 15	9.9 \pm 1.4	12802 \pm 118	5806 \pm 590	...
B057	5 \pm 21	0.03 \pm 0.11	123 \pm 15	1.8 \pm 0.3	7834 \pm 76	849 \pm 87	7.48
B059	26 \pm 8	0.14 \pm 0.05	43 \pm 13	0.7 \pm 0.2	2087 \pm 30	269 \pm 11	5.93
B062	44 \pm 8	0.65 \pm 0.19	116 \pm 13	4.9 \pm 0.8	2554 \pm 32	817 \pm 88	7.14
B064	21 \pm 12	0.20 \pm 0.13	9 \pm 12	0.3 \pm 0.3	1304 \pm 26	289 \pm 31	6.02
B065	8 \pm 6	0.17 \pm 0.15	601 \pm 35	287 \pm 36	5.84
B066	6 \pm 4	0.09 \pm 0.07	103 \pm 12	5.2 \pm 0.7	4536 \pm 47	1866 \pm 86	8.00
B068	107 \pm 24	0.50 \pm 0.16	128 \pm 14	1.7 \pm 0.3	1414 \pm 26	143 \pm 15	5.50
B069	13 \pm 4	0.29 \pm 0.09	801 \pm 58	444 \pm 39	6.20
B070	10 \pm 9	0.15 \pm 0.17	49 \pm 13	2.2 \pm 0.7	1227 \pm 30	421 \pm 60	6.65
B072	12 \pm 3	0.27 \pm 0.08	87 \pm 12	5.9 \pm 0.9	2369 \pm 29	1323 \pm 67	7.78
B073	-31 \pm 18	-0.19 \pm 0.09	41 \pm 13	0.7 \pm 0.3	5195 \pm 33	688 \pm 73	7.20
B075	9 \pm 11	0.09 \pm 0.12	10364 \pm 57	2276 \pm 238	8.57
B076	10 \pm 6	0.17 \pm 0.13	591 \pm 33	227 \pm 26	...
B077	-12 \pm 20	-0.06 \pm 0.10	1098 \pm 25	124 \pm 13	5.33
B079	4576 \pm 71	36.27 \pm 3.92	23326 \pm 213	533.0 \pm 55.8	123665 \pm 436	21333 \pm 2220	9.35
B080	13 \pm 6	0.11 \pm 0.05	118 \pm 17	3.0 \pm 0.4	6379 \pm 36	1335 \pm 44	7.59
B081	268 \pm 13	2.54 \pm 0.37	200 \pm 10	5.5 \pm 0.7	865 \pm 29	178 \pm 19	4.97
B082	10 \pm 14	0.09 \pm 0.14	160 \pm 22	4.2 \pm 0.8	6608 \pm 69	1317 \pm 162	7.08
B083	2 \pm 11	0.02 \pm 0.12	850 \pm 35	196 \pm 22	5.89
B085	157 \pm 23	0.87 \pm 0.21	107 \pm 30	1.7 \pm 0.5	685 \pm 28	82 \pm 9	4.68
B087	26 \pm 18	0.15 \pm 0.12	62 \pm 11	1.1 \pm 0.3	3008 \pm 30	412 \pm 43	6.40
B088	6 \pm 5	0.05 \pm 0.05	35 \pm 11	0.9 \pm 0.3	1404 \pm 28	290 \pm 11	6.05
B089	7 \pm 11	0.06 \pm 0.11	14 \pm 10	0.4 \pm 0.3	763 \pm 32	154 \pm 17	5.58
B091	5 \pm 14	0.04 \pm 0.11	22 \pm 12	0.5 \pm 0.3	425 \pm 33	70 \pm 9	4.88
B092	13 \pm 7	0.22 \pm 0.14	685 \pm 50	275 \pm 35	6.06
B093	150 \pm 16	1.14 \pm 0.26	51919 \pm 182	8571 \pm 1054	9.66
B094	75 \pm 30	0.26 \pm 0.13	163 \pm 14	1.6 \pm 0.3	4321 \pm 47	326 \pm 34	6.38
B096	7 \pm 8	0.10 \pm 0.12	35 \pm 9	1.5 \pm 0.5	793 \pm 26	269 \pm 30	5.94
B098	32 \pm 14	0.27 \pm 0.14	53 \pm 14	1.3 \pm 0.4	576 \pm 23	104 \pm 12	4.82
B100	1 \pm 6	0.03 \pm 0.12	1318 \pm 27	627 \pm 71	...
B101	-38 \pm 18	-0.22 \pm 0.08	717 \pm 26	68 \pm 8	5.34
B102	12 \pm 7	0.12 \pm 0.07	1656 \pm 26	385 \pm 21	6.24

TABLE 5 — *Continued*

No.	4.5 μm		8.0 μm		24 μm		K-[24]
	Excess (μJy)	Ratio ^a	Excess (μJy)	Ratio ^a	Excess (μJy)	Ratio ^a	
B103	47 \pm 25	0.20 \pm 0.12	77 \pm 13	0.9 \pm 0.2	859 \pm 32	79 \pm 9	4.78
B104	31 \pm 26	0.13 \pm 0.12	82 \pm 14	1.0 \pm 0.2	644 \pm 32	56 \pm 6	4.47
B105 ^b	35 \pm 33	0.11 \pm 0.12	26 \pm 18	0.2 \pm 0.2	2664 \pm 30	172 \pm 18	5.85
B107 ^b	-101 \pm 30	-0.36 \pm 0.07	126 \pm 18	1.3 \pm 0.3	1954 \pm 30	149 \pm 16	5.43
B108	2 \pm 11	0.03 \pm 0.18	7551 \pm 53	2580 \pm 280	8.48
B109	-8 \pm 6	-0.21 \pm 0.13	1466 \pm 24	790 \pm 117	...
B112	-8 \pm 15	-0.06 \pm 0.11	55 \pm 17	1.2 \pm 0.4	1654 \pm 28	272 \pm 30	6.27
B115	37 \pm 6	0.45 \pm 0.09	68 \pm 19	2.5 \pm 0.7	4379 \pm 36	1322 \pm 51	7.63
B116	9 \pm 6	0.19 \pm 0.14	636 \pm 34	295 \pm 36	...
B117	-10 \pm 10	-0.11 \pm 0.10	497 \pm 34	111 \pm 14	5.29
B118	24 \pm 9	0.31 \pm 0.15	1267 \pm 26	387 \pm 41	6.41
B119	156 \pm 30	0.56 \pm 0.16	149 \pm 15	1.5 \pm 0.3	889 \pm 30	69 \pm 8	4.38
B122	28 \pm 6	0.27 \pm 0.06	1357 \pm 24	321 \pm 14	6.27
B123	12 \pm 14	0.10 \pm 0.12	761 \pm 25	137 \pm 15	5.55
B124	-2 \pm 10	-0.02 \pm 0.11	621 \pm 34	165 \pm 20	5.50
B125	7 \pm 11	0.08 \pm 0.13	1462 \pm 29	350 \pm 37	6.64
B126	5 \pm 20	0.03 \pm 0.11	17 \pm 13	0.3 \pm 0.2	652 \pm 31	76 \pm 9	4.94
B127	262 \pm 21	1.41 \pm 0.25	199 \pm 12	3.1 \pm 0.4	1433 \pm 27	168 \pm 18	5.70
B128	11 \pm 6	0.09 \pm 0.05	66 \pm 13	1.6 \pm 0.3	2705 \pm 33	533 \pm 18	6.69
B129	8 \pm 8	0.11 \pm 0.12	106 \pm 16	4.0 \pm 0.8	2463 \pm 29	710 \pm 75	7.06
B132	20 \pm 9	0.27 \pm 0.15	164 \pm 20	6.2 \pm 1.1	12811 \pm 87	3669 \pm 387	8.99
B135	20 \pm 5	0.20 \pm 0.06	56 \pm 12	1.7 \pm 0.4	2990 \pm 35	742 \pm 27	7.07
B136	118 \pm 9	2.49 \pm 0.41	65 \pm 11	4.1 \pm 0.9	578 \pm 31	289 \pm 35	5.30
B137	10 \pm 21	0.05 \pm 0.11	19 \pm 14	0.3 \pm 0.2	746 \pm 25	82 \pm 9	4.84
B139	7 \pm 3	0.15 \pm 0.08	38 \pm 10	2.6 \pm 0.7	1521 \pm 26	850 \pm 46	...
B140	97 \pm 9	1.49 \pm 0.28	63 \pm 13	2.8 \pm 0.7	672 \pm 62	225 \pm 32	5.53
B141	629 \pm 14	6.20 \pm 0.98	9717 \pm 50	276.3 \pm 37.9	136366 \pm 514	29269 \pm 3996	10.93
B142	20 \pm 7	0.11 \pm 0.05	28 \pm 13	0.5 \pm 0.2	2986 \pm 32	421 \pm 14	6.35
B144	11 \pm 4	0.14 \pm 0.06	77 \pm 15	3.0 \pm 0.6	2606 \pm 35	832 \pm 31	7.33
B145	10 \pm 4	0.16 \pm 0.07	169 \pm 11	8.2 \pm 0.6	3905 \pm 49	1544 \pm 65	7.52
B148	7 \pm 14	0.05 \pm 0.11	41 \pm 15	0.9 \pm 0.4	922 \pm 27	165 \pm 18	5.50
B152	4 \pm 5	0.04 \pm 0.05	2813 \pm 29	649 \pm 22	7.01
B154	37 \pm 7	0.85 \pm 0.27	1414 \pm 29	702 \pm 101	...
B156	38 \pm 7	0.22 \pm 0.05	67 \pm 17	1.2 \pm 0.3	2456 \pm 32	347 \pm 11	6.12
B159	1 \pm 10	0.01 \pm 0.11	23 \pm 9	0.7 \pm 0.3	1299 \pm 28	324 \pm 35	6.27
B160	21 \pm 3	0.44 \pm 0.09	225 \pm 12	14.5 \pm 1.1	9941 \pm 62	5216 \pm 249	8.42
B161	1 \pm 6	0.02 \pm 0.12	2090 \pm 35	890 \pm 96	...
B163	10 \pm 5	0.12 \pm 0.06	132 \pm 11	4.7 \pm 0.5	5637 \pm 45	1645 \pm 72	7.97
B165	27 \pm 19	0.16 \pm 0.12	44 \pm 14	0.7 \pm 0.3	1347 \pm 28	166 \pm 18	5.49
B167	-18 \pm 15	-0.13 \pm 0.09	1076 \pm 55	94 \pm 11	6.13
B169	12 \pm 4	0.18 \pm 0.07	1086 \pm 26	392 \pm 20	6.46
B172	37 \pm 7	0.81 \pm 0.22	535 \pm 33	259 \pm 33	...
B175 ^b	22 \pm 6	0.51 \pm 0.18	1007 \pm 27	507 \pm 58	...
B177	11 \pm 3	0.30 \pm 0.10	1629 \pm 41	1046 \pm 63	...
B179 ^b	3 \pm 16	0.02 \pm 0.11	2321 \pm 29	362 \pm 38	6.33
B182	17 \pm 24	0.07 \pm 0.11	48 \pm 15	0.6 \pm 0.2	1090 \pm 24	112 \pm 12	5.04
B183	36 \pm 8	0.28 \pm 0.07	237 \pm 14	5.4 \pm 0.4	12674 \pm 169	2370 \pm 99	8.16
B184	1 \pm 12	0.01 \pm 0.13	707 \pm 37	166 \pm 21	5.49
B188	-5 \pm 9	-0.05 \pm 0.11	3046 \pm 30	783 \pm 83	7.45
B190	280 \pm 46	0.65 \pm 0.17	301 \pm 20	2.0 \pm 0.3	597 \pm 27	30 \pm 3	3.39
B191	697 \pm 24	3.98 \pm 0.67	5744 \pm 39	94.4 \pm 12.9	135114 \pm 689	16765 \pm 2269	10.33
B192	5 \pm 17	0.03 \pm 0.11	954 \pm 25	133 \pm 14	5.45
B193	13 \pm 12	0.12 \pm 0.12	1014 \pm 26	218 \pm 23	5.77

^a Ratio is measured excess divided by expected photosphere.^b Detected at 70 μm .

TABLE 6
DUST PARAMETERS FOR SMC STARS WITH SECURE SPECTRAL TYPES AND
MEASURABLE 8 MICRON EXCESS

Object ID	SpT	T (K)	Mass (M_{\oplus})	F_{IR}/F_{Bol} ($\times 10^{-3}$)	R_{BB} ^a (au)	R_{MBB} ^a ($\times 10^4$ au)	a_{min} (mm)	M_{bo} ^b (M_{\oplus})
B021	B0	135^{+4}_{-4}	$0.17^{+0.05}_{-0.04}$	$0.42^{+0.31}_{-0.17}$	954^{+124}_{-256}	2.3	0.5	13
B022	B0	132^{+1}_{-1}	$1.08^{+0.23}_{-0.21}$	$2.30^{+2.01}_{-0.97}$	994^{+89}_{-261}	2.5	0.5	80
B023	O7	127^{+0}_{-1}	$8.25^{+1.67}_{-1.57}$	$3.28^{+0.89}_{-0.98}$	2211^{+192}_{-168}	5.8	1.3	1689
B029	B0	118^{+3}_{-3}	$1.82^{+0.49}_{-0.37}$	$1.95^{+1.38}_{-0.80}$	1248^{+130}_{-353}	3.5	0.5	134
B042	B0	136^{+1}_{-1}	$1.12^{+0.23}_{-0.21}$	$2.88^{+2.34}_{-1.16}$	933^{+78}_{-254}	2.3	0.5	82
B043	O9	125^{+3}_{-4}	$0.71^{+0.19}_{-0.15}$	$0.57^{+0.30}_{-0.17}$	1526^{+128}_{-240}	4.0	0.8	83
B047	O7	129^{+2}_{-2}	$0.70^{+0.16}_{-0.13}$	$0.31^{+0.08}_{-0.09}$	2144^{+195}_{-183}	5.5	1.3	144
B048	B2	128^{+3}_{-4}	$0.58^{+0.14}_{-0.12}$	$7.94^{+3.35}_{-4.01}$	380^{+92}_{-64}	1.0	0.1	10
B059	O9	128^{+3}_{-5}	$0.43^{+0.13}_{-0.07}$	$0.39^{+0.18}_{-0.12}$	1470^{+127}_{-229}	3.8	0.8	50
B064	B0	115^{+11}_{-9}	$0.46^{+0.23}_{-0.18}$	$0.42^{+0.37}_{-0.16}$	1316^{+138}_{-427}	3.8	0.5	34
B066	O9	129^{+2}_{-2}	$0.88^{+0.19}_{-0.17}$	$0.86^{+0.41}_{-0.25}$	1438^{+104}_{-234}	3.7	0.8	104
B072	O8.5	136^{+2}_{-2}	$0.36^{+0.08}_{-0.07}$	$0.39^{+0.11}_{-0.12}$	1432^{+130}_{-121}	3.5	0.9	49
B073	B1	116^{+3}_{-4}	$1.73^{+0.58}_{-0.37}$	$5.63^{+3.33}_{-1.95}$	705^{+78}_{-141}	2.0	0.2	54
B080	O8.5	127^{+2}_{-2}	$1.38^{+0.29}_{-0.26}$	$0.95^{+0.29}_{-0.29}$	1665^{+166}_{-143}	4.4	0.9	187
B082	B1	130^{+2}_{-2}	$1.25^{+0.29}_{-0.22}$	$8.13^{+4.72}_{-2.60}$	559^{+48}_{-108}	1.4	0.2	39
B087	B0	128^{+2}_{-4}	$0.61^{+0.13}_{-0.12}$	$1.08^{+0.88}_{-0.45}$	1059^{+100}_{-307}	2.7	0.5	45
B088	O7	131^{+4}_{-5}	$0.26^{+0.09}_{-0.06}$	$0.12^{+0.03}_{-0.04}$	2095^{+255}_{-202}	5.3	1.3	53
B089	B1	126^{+8}_{-8}	$0.17^{+0.08}_{-0.05}$	$0.90^{+0.54}_{-0.30}$	598^{+86}_{-136}	1.6	0.2	5
B096	B0	139^{+4}_{-4}	$0.11^{+0.03}_{-0.02}$	$0.32^{+0.24}_{-0.13}$	893^{+100}_{-242}	2.1	0.5	8
B098	B1	153^{+5}_{-6}	$0.05^{+0.02}_{-0.01}$	$0.93^{+0.50}_{-0.32}$	407^{+45}_{-83}	0.9	0.2	2
B105 ^c	B2	118^{+7}_{-8}	$0.80^{+0.41}_{-0.23}$	$6.69^{+2.80}_{-3.39}$	448^{+119}_{-89}	1.3	0.1	14
B107 ^c	B1	146^{+2}_{-3}	$0.22^{+0.05}_{-0.04}$	$2.88^{+1.58}_{-1.02}$	445^{+38}_{-85}	1.0	0.2	7
B126	B1	131^{+9}_{-10}	$0.12^{+0.06}_{-0.04}$	$0.81^{+0.49}_{-0.27}$	552^{+87}_{-124}	1.4	0.2	4
B128	O9	130^{+2}_{-3}	$0.51^{+0.12}_{-0.10}$	$0.52^{+0.27}_{-0.16}$	1413^{+112}_{-215}	3.6	0.8	59
B136	B0	157^{+3}_{-4}	$0.05^{+0.01}_{-0.01}$	$0.29^{+0.23}_{-0.12}$	707^{+86}_{-186}	1.5	0.5	4
B137	B1	131^{+9}_{-10}	$0.14^{+0.08}_{-0.04}$	$0.92^{+0.61}_{-0.31}$	552^{+89}_{-127}	1.4	0.2	4
B139	O9	131^{+3}_{-4}	$0.28^{+0.08}_{-0.06}$	$0.29^{+0.15}_{-0.08}$	1410^{+112}_{-216}	3.6	0.8	33
B142	O8.5	118^{+4}_{-6}	$0.90^{+0.36}_{-0.20}$	$0.42^{+0.11}_{-0.13}$	1909^{+304}_{-197}	5.4	0.9	123
B148	B0	139^{+5}_{-6}	$0.13^{+0.04}_{-0.03}$	$0.37^{+0.30}_{-0.16}$	893^{+110}_{-247}	2.1	0.5	9
B159	B0	126^{+5}_{-6}	$0.29^{+0.10}_{-0.07}$	$0.46^{+0.36}_{-0.19}$	1095^{+129}_{-322}	2.9	0.5	21
B182	B0	139^{+5}_{-5}	$0.15^{+0.05}_{-0.03}$	$0.44^{+0.34}_{-0.18}$	895^{+112}_{-242}	2.1	0.5	11

^a R_{BB} is the distance to the star assuming a blackbody emitter (Eq. 9), R_{MBB} uses the modified blackbody emitter with $\lambda_0 = 1 \mu\text{m}$ (Eq. 10).

^b The mass of dust grains of size a_{min} , calculated from F_{IR}/F_{Bol} using Eq. 13.

^c Has a $70 \mu\text{m}$ detection.

TABLE 7
GAUSTAD AND VAN BUREN DUST PARAMETERS

Object ID	SpT	$T_{12/24}$ (K)	Mass (M_{\oplus})	F_{IR}/F_{Bol} ($\times 10^{-3}$)	R_{BB} ^a (AU)	R_{MBB} ^a ($\times 10^4$ au)	a_{min} (mm)	M_{bo} ^b (M_{\oplus})
HR 533	B1	126	0.20	1.06	593	1.4	0.2	16
HR 1191	B1	139	0.06	0.58	488	1.3	0.2	6
HR 1763	B1	120	5.68	23.17	653	2.0	0.2	426
HR 1798	B2	124	0.07	0.83	408	1.0	0.1	3
HR 1855	B0	107	0.16	0.10	1522	4.6	0.5	23
HR 1868 ^c	B1	124	0.48	2.38	614	1.8	0.2	39
HR 1931	O9	103	2.39	0.58	2278	7.1	0.8	487
HR 2058	B1	108	0.18	0.39	814	2.2	0.2	11
HR 2734	B0	162	0.08	0.61	664	1.2	0.5	27
HR 5993 ^c	B1	137	0.06	0.57	506	1.4	0.2	6
HR 6028 ^c	B2	121	0.10	0.92	428	1.1	0.1	4
HR 6165	B0	145	1.66	6.01	831	1.9	0.5	422
HR 6601	B1	130	0.08	0.52	558	1.3	0.2	7
HR 6788 ^c	B1	115	0.08	0.27	711	2.2	0.2	6
HR 7993	B0	146	0.04	0.16	814	1.7	0.5	11
HR 8047 ^c	B1	150	0.02	0.33	423	1.0	0.2	3
HR 8854 ^c	B0	121	0.77	0.95	1188	3.2	0.5	137

^a R_{BB} is the distance to the star assuming a blackbody emitter (Eq. 9), R_{MBB} uses the modified blackbody emitter with $\lambda_0 = 1 \mu\text{m}$ (Eq. 10).

^b The mass of dust grains of size a_{min} , calculated from F_{IR}/F_{Bol} using Eq. 13.

^c Known reflection nebula.